Radar Sounding of Europa's Subsurface Properties and Processes: The View from Earth

Donald D. Blankenship and Duncan A. Young
University of Texas at Austin

William B. Moore
University of California at Los Angeles

John C. Moore
University of Lapland and University of Oulu

A primary objective of future Europa studies will be to characterize the distribution of shallow subsurface water as well as to identify any ice-ocean interface. Other objectives will be to understand the formation of surface and subsurface features associated with interchange processes between any ocean and the surface as well as regional and global heat flow variations. Orbital radar sounding, a now maturing technology, will be an essential tool for this work. We review the hypothesized processes that control the thermal, compositional, and structural properties, and therefore the dielectric character, of the subsurface of Europa's icy shell. We introduce fundamental concepts in radar sounding and then assess analog processes represented by, and sounded in, Earth's ice sheet. We use these Earth analog studies to define the radar imaging approach for Europa's subsurface that will be most useful for testing the hypotheses for the formation of major features.

1. INTRODUCTION

Europa is a hypothesized site of incipient habitability because of its potentially vast subsurface ocean (see chapter by Hand et al.). The presence of this water reservoir has been inferred indirectly from Europa's induced magnetic field (*Kivelson et al.,* 2000; *Hand and Chyba,* 2007; see also chapter by Khurana et al.) and tectonic mapping of its young surface (*Hoppa et al.,* 1999; *Pappalardo et al.,* 1999; see chapter by Kattenhorn and Hurford). Future space-based geodetic measurements of Europa's time varying gravity field would definitively demonstrate the existence of an ocean. However, understanding this ocean's coupling to its overlying crust — key for understanding Europa's astrobiologic potential — will require sounding Europa's third dimension.

Airborne ice-penetrating radar is now a mature tool in terrestrial studies of Earth's ice sheets (*Bingham and Siegert,* 2007), and orbital examples have been successfully deployed at Earth's Moon and Mars. Recent terrestrial examples include the University of Texas' High Capability Airborne Radar Sounder (HiCARS) (*Peters et al.,* 2005), the British Antarctic Survey's PASIN system (*Heliere et al.,* 2007), and the University of Kansas's IPR and CARDS systems (*Gogineni et al.,* 2001). Spaceborne demonstrations include NASA's Apollo 17 ALSE (*Porcello et al.,* 1974), JAXA's LRS system on the Kaguya lunar orbiter (*Ono et al.,* 2008), MARSIS onboard ESA's Mars Express (*Picardi et al.,* 2005), and SHARAD onboard NASA's Mars Reconnaissance Orbiter (*Seu et al.,* 2007). In this chapter we briefly review the target of observations, Europa's ice crust and the ocean that likely lies beneath; summarize the state of the art of radar-sounding systems; survey previous observations made by ice-penetrating radar at Earth; and examine the challenge of operating such a system at Europa.

The key to probing Europa's subsurface lies in the relatively large ratio (the loss tangent, τ) between the real and imaginary components of the electrical permittivity (ε) of water ice (i.e., the ice is a good insulator). Instead of losing energy in coupling with ions and electrically charged defects in the ice lattice structure within the medium, propagating electromagnetic waves can penetrate far into an ice column (*Gudmandsen,* 1971; *Petrenko and Whitworth,* 1999). For frequencies between 1 and 300 MHz, the loss tangent of pure water ice does not vary significantly for a given temperature (*Fujita et al.,* 1993; *MacGregor et al.,* 2007). However, with increasing temperatures and/or contamination, crystal defects and ions increase in number and mobility, and above eutectic temperatures water veins with high impurity content may start to play a role in increasing the conductivity of the ice, absorbing more of the radar wave energy.

Liquid water containing impurities (brine) is an effective conductor of electricity, and hence strongly dissipates electromagnetic energy. In addition, strong contrast in real permittivity at radio frequencies between pure water ice ($\varepsilon \sim 3.15$) and liquid water [$\varepsilon \sim 80$ (*Peters et al.,* 2005; *Campbell,* 2002)] lead to a large dielectric impedance contrast that typically results in a highly reflective interface, with a reflection of half or more the incident power, compared to

a thousandth of the incident power reflected by silicate rock. It is this strong contrast that enables exploration for water within Europa's crust.

Our foundation for this chapter will be the hypothesized processes that control the thermal, compositional, and structural (TCS) properties, and therefore the dielectric character, of the subsurface of Europa's icy shell. We will begin by reviewing the processes that may affect TCS properties in Europa's icy shell. This includes thermochemical and mechanical processes that have been linked to observable features at the surface of Europa. Sounding of the TCS properties of the shell may thus be used to test hypotheses for the origin of these features and the evolution of the icy shell. Many of these processes have direct analogs in terrestrial ice sheets. We then introduce basic concepts and methods used in radar sounding of ice, including procedures used to improve range, power, and azimuth resolution. We will then review the spectrum of analog processes and TCS properties represented by Earth's icy bodies including both Arctic and Antarctic ice sheets, ice shelves, and valley glaciers. There will be few complete analogs over the full TCS space, but there are more analog examples than one might imagine for significant portions of this space (e.g., bottom crevasses, marine ice shelf/subglacial lake accretion, surging polythermal glaciers). Our final contribution will be to use the Earth analog studies to describe the radar imaging approach for Europa's subsurface that will be most useful for supporting/refuting the hypotheses for the formation of major surface/subsurface features as well as for "pure" exploration of Europa's icy shell and its interface with the underlying ocean.

2. STRUCTURAL, COMPOSITIONAL, AND THERMAL PROPERTIES OF EUROPA'S ICY SHELL

Europa's icy shell has a geologically young surface that records less than about 100 m.y. of impacts (*Zahnle et al.,* 2003; chapter by Beirhaus et al.), and which shows abundant evidence of modification by endogenic processes. Particularly evident are fractures, primarily strike-slip with some extensional features (bands) (see chapters by Kattenhorn and Hurford, and by Prockter and Patterson). There are a small number of impact craters ranging up to 50 km in diameter (see chapter by Schenk and Turtle). Finally, there are a number of features collectively referred to as lenticulae, but plausibly including chaos regions of all sizes, that have been suggested to be due to thermal modification of the near surface by convective (*Pappalardo et al.,* 1998, *Nimmo and Manga,* 2002) or melt-through (*Greenberg et al.,* 1999) processes (see chapter by Collins and Nimmo). There are a number of candidate processes for producing dielectric horizons within these structures, most of which have good terrestrial analogs. This section will describe what we might expect a radar sounder to be able to reveal about these processes and what sorts of structures we would expect to see. Ultimately, we seek to test hypotheses related to the origin of these structures and their implications for the evolution of Europa's ocean and icy shell.

Four classes of processes are considered: marine, convective, tectonic, and impact.

2.1. Marine Processes

A "marine" europan crust could be formed by processes similar to those for ice that accretes beneath the large ice shelves of Antarctica where frazil ice crystals form directly in the ocean water (*Moore et al.,* 1994). This model is characterized by slow accretion (freezing) or ablation (melting) on the lower side of the icy crust (*Greenberg et al.,* 1999). Impurities present in the ocean tend to be rejected from the ice lattice during the slow freezing process. Temperature gradients for a "marine" ice model are primarily a function of ice thickness and the temperature/depth profile is described by a simple diffusion equation for a conducting ice layer (*Chyba et al.,* 1998). The low-temperature gradients at any ice water interface, combined with impurity rejection from accreted ice, would likely lead to significant dielectric horizons resulting from contrasts in ice crystal fabric and composition. Similarly, the melt-through hypothesis for the formation of lenticulae and chaos on Europa's surface implies that ice will accrete beneath the feature after it forms. This process will result in a sharp boundary between old ice (or rapidly frozen surface ice) and the deeper accreted ice. The amount of accreted ice would be directly related to the time since melt-through occurred and could be compared with the amount expected based on the surface age.

Testing these hypotheses will require measuring the depth of interfaces to a resolution of a few hundred meters, and horizontal resolutions of a fraction of any lid thickness, i.e., a kilometer or so.

2.2. Convective Processes

The thermal structure of the shell (apart from local heat sources) is set by the transport of heat from the interior (see chapter by Barr and Showman). Regardless of the properties of the shell or the overall mechanism of heat transport, the uppermost several kilometers is thermally conductive, cold, and stiff. The thickness of this conductive "lid" is set by the total amount of heat that must be transported and thus a measurement of the thickness of the cold and brittle part of the shell is a powerful constraint on the heat production in the interior. This uppermost part of the shell has experienced continuous input of impurities to the surface that are gradually mixed downward through impact gardening.

The lower, convecting part of the shell (if it exists) is likely to be much cleaner, because regions with impurities should have experienced melting at some point during convective circulation (when the material was brought near the base of the shell) and the melt will segregate downward efficiently, extracting the impurities from the shell (*Pappalardo and Barr,* 2004). Convective instabilities also result

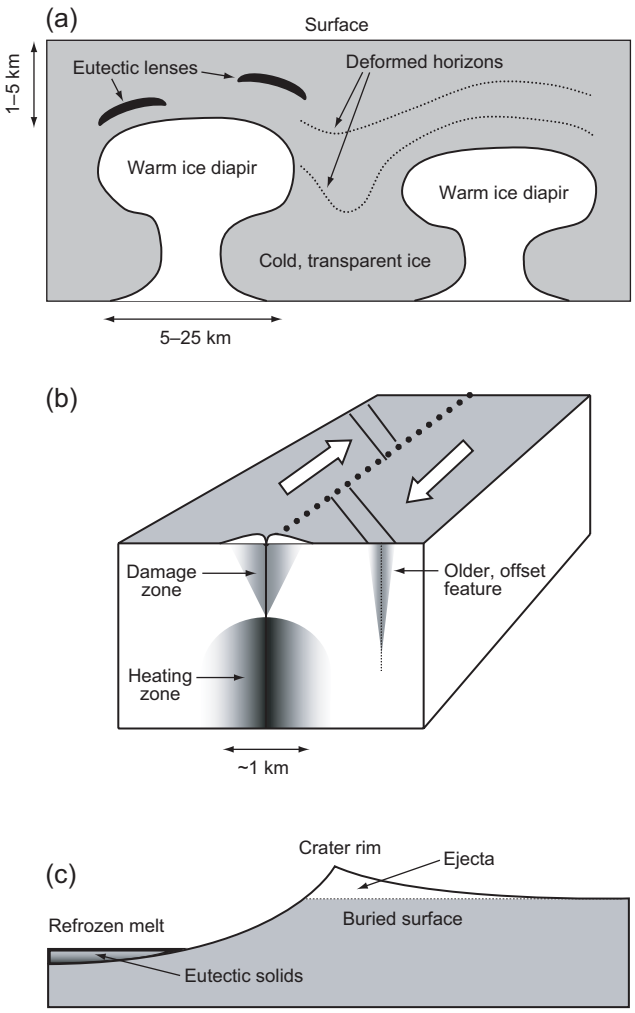

Fig. 1. Illustrations of some of the processes leading to thermal, compositional, and structural horizons in Europa's icy shell. **(a)** Convective diapirs causing thermal perturbations and potentially melting in the overlying rigid ice. **(b)** Tectonic faulting driven by tidal stresses resulting in fault damage and frictional heating. **(c)** An impact crater with a refrozen melt pool at its center and the surrounding ejecta blanket.

in thermal variations in the outer part of the shell (the rigid lid in convective parlance) that may be measured (Fig. 1a). The scale of these instabilites is on the order of hundreds of kilometers, independent of the thickness of the shell, and the temperature variations will be a few tens of Kelvin (*Nimmo and Manga,* 2002). Convective structures would arise through ductile deformation of other horizons (impact or tectonic), or through the effect of these thermal anomalies, which may lead to local regions or highly dissipative (or conversely, highly transparent) ice or even eutectic melting.

A number of features at the surface of Europa (lenticulae and chaos), with scales ranging from 1 km to hundreds of kilometers have been associated with thermal perturbations of the shell (convective or melt-through as described above) (*Pappalardo et al.,* 1998; *Greenberg et al.,* 1999; *Nimmo and Manga,* 2002). When warm, relatively pure ice diapirs from the interior approach the surface, they may be far from the pure-ice melting point, but may be above the eutectic point of many substances, and may therefore create regions of melting within the rigid shell above them as the temperature increases above the flattening diapir (Fig. 1a). The dielectric horizon associated with these melt regions would provide a good measurement of the thickness of the conductive layer.

Given that the cutoff length scale is a key discriminator between models for the formation of lenticulae and chaos (*Pappalardo et al.,* 1998; see chapter by Collins and Nimmo), high horizontal resolution (a few hundred meters) is required to avoid scale-related biases. The ability to sound through regions of rough large-scale terrain will also be essential. Detection of water lenses would require a vertical resolution of at least a few tens of meters.

2.3. Tectonic Processes

Europa's surface is extensively fractured and modified by tectonic processes (see chapters by Kattenhorn and Hurford and by Prockter and Patterson). Many of the offsets are horizontal, but some extensional features (e.g., bands) are seen. Large-scale arcuate troughs form a globally organized pattern (*Schenk et al.,* 2008) that may relate to true polar wander. Limited evidence for contractional tectonism has been inferred. This is a unique tectonic regime in the solar system, and the processes controlling the distribution of strain in Europa's icy shell are uncertain. The ubiquitous double-ridges are commonly associated with strike-slip offset, and the origin of the topography of these features remains debated.

Tectonic processes may result in subsurface structures characterized by rapid freezing of water injected into fracture zones (*Greenberg et al.,* 1998). The large temperature gradients implied by this process could lead to ice with properties similar to terrestrial sea ice (*Weeks et al.,* 1990), although water reaching the surface would be unlike sea ice because of very rapid boiling. Because fractures that extend through the shell require a thin shell, this model would also be characterized by a temperature/depth profile for a simple thermally conducting ice layer.

Other tectonic structures could range from subhorizontal extensional fractures to near-vertical strike-slip features, and will produce dielectric horizons associated with primarily with the faulting process itself through formation of pervasively fractured ice, and zones of deformational melt, injection of water, or preferred orientation of crystalline fabric. Some faults may show dielectric contrasts by local alteration including fluid inclusions or simply by juxtaposition of dissimilar regions including offset of preexisting structures through motion on the fault.

While faulting may create dielectric contrasts by relative motion juxtaposing different terrains on either side of the fault, the tidal stress environment of Europa may lead to continuously active faults and significant thermal modification

of the ice around the fault (Fig. 1b). Such processes may lead to melting and potentially to communication with the ocean from above. In one model for the triple bands (*Nimmo and Gaidos,* 2002), the double-ridge structure is generated by thermal buoyancy due to frictional heating along the fault. The dielectric structure implied by this model would include a broad region of warm, dissipative ice extending several kilometers on either side of the fault. At the fault surface itself, melt may be generated, which will flow downward. This structure may vary along the fault according to the orientation of the fault relative to the tidal stress field.

There are a number of outstanding questions regarding these tectonic features. A measurement of their depth extent and association with thermal anomalies would strongly constrain models of their origins. In particular, correlation of subsurface structure with surface properties (length, position in the stratigraphic sequence, height and width of the ridges) will test hypotheses for the mechanisms that form the fractures and support the ridges. The observation of melt along the fracture would make these features highly desirable targets for future *in situ* missions.

Extensional structures observed on Europa (bands) have been likened to oceanic spreading centers on Earth (see chapter by Prockter and Patterson). The bookshelf normal faulting known from the Earth case is plausibly responsible for the observed surface morphology of the europan features. These faults are shallow, with depths comparable to their spacing (a few kilometers) and offsets several times less than this (a few hundred meters). Any preexisting layering should be broken up and tilted within each block, but if the analogy with spreading centers is accurate, the material in the band is newly supplied from below and may not have any preexisting horizons. In either case, material must be supplied from below and may have a distinct dielectric signature. The origin of the material in the bands may thus be constrained by sounding the subsurface structure. Bands and ridges typically have length scales of a few kilometers. Horizontal resolutions a factor of 10 higher than this would be required to fully diagnose processes. For extensional structures, the ability to image structures sloping more than a few degrees is also necessary. Again, tens of meters of vertical resolution would be required to image near-surface water.

2.4. Impact Processes

The impact process represents a profound disturbance of the local structure of the shell (see chapter by Schenk and Turtle). Around the impact site, the ice is fractured and heated, and some melt is generated. The surface around the impact is buried to varying degrees with a blanket of ejecta. Finally, the relaxation of the crater creates a zone of tectonism that can include both radial and circumferential faulting. These processes all create subsurface structures that may be sounded electromagnetically. An outstanding mystery on Europa is the process by which old craters are erased from the surface. It may be possible to find the subsurface signature of impacts that are no longer evident at the surface, which would place constraints on the resurfacing processes that operate at Europa.

Impact processes affect the structure of the icy shell to different extents depending on the size of the impactor, and it is possible that Europa's subsurface records events that have penetrated the entire thickness of the shell (at the time). Three types of dielectric horizons are expected to be derived from impact: the former surface buried beneath an ejecta blanket, solidified eutectics in the impact structure itself, and impact-related fractures (e.g., a ring graben).

The surface gradually accumulates contaminants from Jupiter orbit, mostly from Io, but also from micrometeorite impact (*Eviatar et al.,* 1981; *McEwen,* 1986). These micrometeorites also gradually mix the uppermost few meters of the ice in a process known as impact gardening. When a larger impact occurs, this surface layer is buried by many meters of ice derived from deeper and presumably cleaner regions (Fig. 1c). Thus a dielectric discontinuity is created between the ejecta blanket and the old surface. This horizon will be nearly horizontal (some postimpact deformation is expected as the crater relaxes) and should be sharp, because the contaminants accumulate most strongly in the top tens of centimeters. The horizon should approach the surface as the distance from the crater increases.

Multiple, overlapping ejecta blankets may create a complexly layered structure, with several subhorizontal horizons at different depths. This type of structure is similar to that produced by interlayering of snow and ice with volcanic deposits in terrestrial ice sheets. Europa has very few obvious craters, but if the process that removes them is surficial (e.g., shallow tectonic reworking), the deep structures created by previous impacts may be preserved. On the other hand, if the resurfacing process involves the entire shell thickness (melt-through), then such structures will be erased as well. Subsurface sounding will make it possible to test hypotheses for the processes that govern resurfacing on Europa.

In the center of the impact crater, melt will be produced, which will pool at the base of the crater and then freeze out rapidly (Fig. 1c). The melt pool will contain the impurities initially in the ice that was molten during the impact, but as it freezes, the impurities in the pool will concentrate, and various eutectics will be reached depending on the initial composition. We can thus expect a vertically and concentrically layered structure of ice and eutectic compositions with a sharp transition (a few centimeters) between relatively pure ice and the first eutectic solid. Subsequent relaxation of the crater may deform this structure vertically, creating a domed, concentrically zoned structure. A central peak, if formed, would result in an initially ring-shaped melt pool and subsequent rings of eutectic zonation.

Radial fractures near the crater accommodate relatively little motion, but the possibility of melt injection along these fractures (as seen in the Sudbury and Vredefort structures on Earth) may create very strong dielectric contrasts as described above. These structures will be nearly vertical and

may extend downward beneath the impact crater itself as well as radially away from the center. The injected dikes may be up to several meters wide near the impact structure and will gradually thin with distance, depending on the size of the impact. The melt will freeze quickly once it has traveled away from the strongly heated region near the crater and may contain enhanced levels of impurities because some water may have been lost during the impact event itself. If sufficient melt is produced, the circumferential fractures may also become melt filled, or melt may be produced by friction along the circumferential fractures during the rapid collapse of the transient crater (analogous to the pseudotachlyte zones associated with the Sudbury structure).

Finally, tectonics is also driven by the impact process. As mentioned above, the large-scale concentric fractures observed on several icy bodies may offset preexisting horizons by hundreds of meters. The scale of motion on these features can be large, up to several kilometers on the largest features (*Moore et al.,* 1998). Although subvertical near the surface, these features are predicted to flatten with depth, and may preferentially sole out into preexisting horizons, a hypothesis that may be tested by sounding.

Vertical resolutions on the scales of a few tens to hundreds of meters will be required to identify ejecta blankets. Detection of at least the edges of steep interfaces would aid in the identification of radial dikes, buried crater walls, and circumferential fractures.

3. FUNDAMENTALS OF RADAR SOUNDING

Radar systems are active remote sensing systems that operate by transmitting an electromagnetic pulse at a given time (t_t) and receiving an echo at a later time (t_r). For a monostatic system, where the transmitting and receiving elements are collocated, the range (r) to the target will be

$$r = c\frac{(t_r - t_t)}{2}$$

where c is the speed of light in the material between the transmitter and the target (Fig. 2). For sounding through ice, the range will be

$$r = c\,\frac{\left((t_{surface} - t_t) + (t_{bed} - t_{surface})/n_{ice}\right)}{2}$$

where $t_{surface}$ is the time of the surface echo, t_{bed} is the time of the basal echo, and n_{ice} is the refractive index of ice. The reflection radar equation for power received for a specular interface, monostatic system, and transmission through free space is

$$P_r = P_t : \left(\frac{\lambda}{4\pi}\right)^2 : \frac{G^2 R_{01}}{(2r)^2} \qquad (1)$$

where P_r is the power received, P_t is the power transmitted, λ is the wavelength of the carrier wave, G is the gain (the "focusing") due to the antenna, and R_{01} is the effective reflection coefficient of the surface.

Electromagnetic radiation interacts with surfaces in a number of ways; it can reflect off of a surface flat at wavelength scales, it can scatter off wavelength scale diffractors, and it can be transmitted through the surface. While the scattering radar equation uses an r^4 term [e.g., used for side-looking SAR imaging and observatory-based planetary radar systems (*Campbell,* 2002; *Stiles et al.,* 2006)] with which many may be familiar, the surface return from a nadir-pointed system can be treated as that of a mirrored transmitter, as in the above equation. The implication of this equation is that the inverse square law will reduce the received power, while the gain of the antenna will boost it.

This process is repeated as fast as the travel time will allow as the platform moves along its track. For sounding systems, the resulting waveform records (after processing and coding of intensity) are used as columns in depth profiles known as radargrams (e.g., Figs. 2 and 3). Important parameters in detecting and interpreting these echoes include the system's *signal to noise ratio* (SNR, which represents signal quality and dictates the depth of penetration), its *bandwidth* (which controls the radar's range resolution and hence the vertical resolution of a radargram), its *beam pattern* (which determines the radar's azimuthal resolution and hence the horizontal resolution), and its *center frequency* (which determines its sensitivity to the size of structures and the depth of penetration).

3.1. Signal Quality and Vertical Range Resolution

The first two parameters, SNR and bandwidth, are linked. The SNR is the comparison between the power of the echo of interest and the power from all other sources. Given the large dynamic range of radar receivers, and the geometrically controlled exponential decay rates of radar energy, it is convenient to use a logarithmic scale for expressing power ratios. We use deciBels [i.e., dB; $10\log_{10}\left(\frac{power1}{power2}\right)$] to discuss the ratio of two powers, and similarly use dBm to compare absolute power to a 1 mW reference.

Bandwidth (BW), measured in Hertz, is the range of frequencies over which the system responds. The vertical range resolution for a nadir-pointed system that is implied by a given bandwidth is

$$\delta r = \frac{c}{2BWn_{ice}}$$

Bandwidth is often much lower than the system's center frequency. Higher bandwidth means that the system is capable of resolving smaller time intervals, and hence, smaller range differences. A simple way of generating a received echo with wide inherent bandwidth is to transmit a very short pulse. However, this approach limits the total energy a pulse can carry, and thus reduces the likelihood of detection above electronic noise in the receiver. A long pulse with

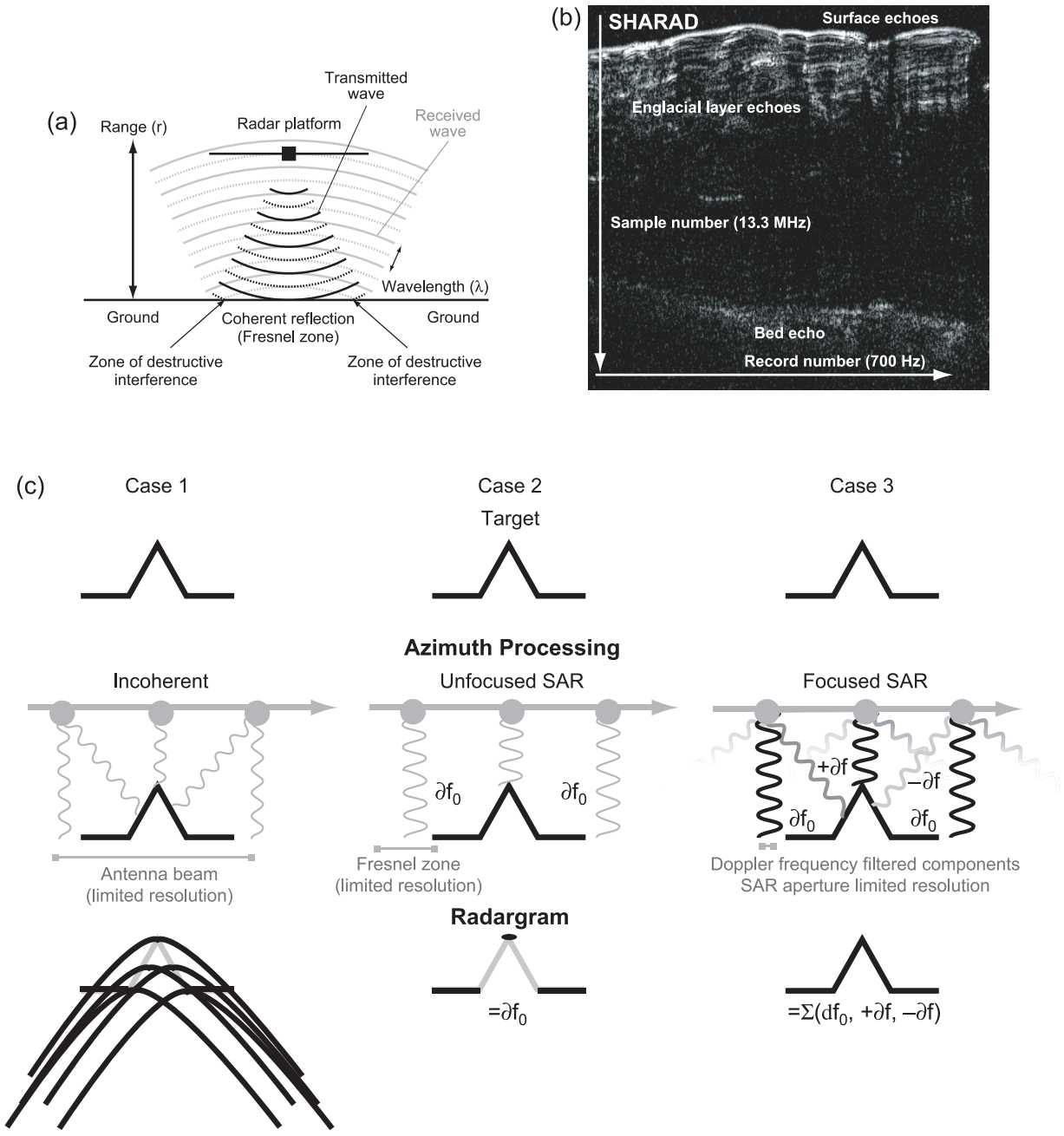

Fig. 2. **(a)** Illustration of the typical geometry of an air- or spaceborne radar altimeter or sounder, illustrating the concept of the Fresnel zone — a region over which adjacent reflecting spots on a flat surface reenforce. **(b)** Example radargram from the SHARAD instrument penetrating Mars' north polar layered deposits, from MRO orbit 1957. Each column of the radargram represents a separate time series sampling the reflected radio pulse. **(c)** Schematic view of the effects of different along-track processing methods on radar sounding. Case 1 shows incoherent processing, where the phase of the signal is ignored and only the total power is considered. Case 2 shows unfocused SAR, which is effectively filtered so that only reflections with zero Doppler shift are passed. Case 3 shows focused SAR, where effectively beams of different Doppler frequency are separated out and recombined at high angular resolution.

narrow bandwidth can contain more total energy and will be more easily detected, but will poorly resolve the target range.

A solution to this conflict has been to use "chirped" pulses, where the frequency is swept across the desired bandwidth with specific phase, over an extended pulse length. The received extended echo is "pulse compressed" through convolution with the original signal, to return the resolution implied by the bandwidth. A side effect of pulse compression are low-amplitude "sidelobes" preceding and following the real echo. In the example of the SHAllow RADar (SHARAD) system on the Mars Reconnaissance Orbiter (*Seu et al.,* 2007) (Fig. 2), pulse compression yields a 27.5-dB power enhancement over a conventional pulse

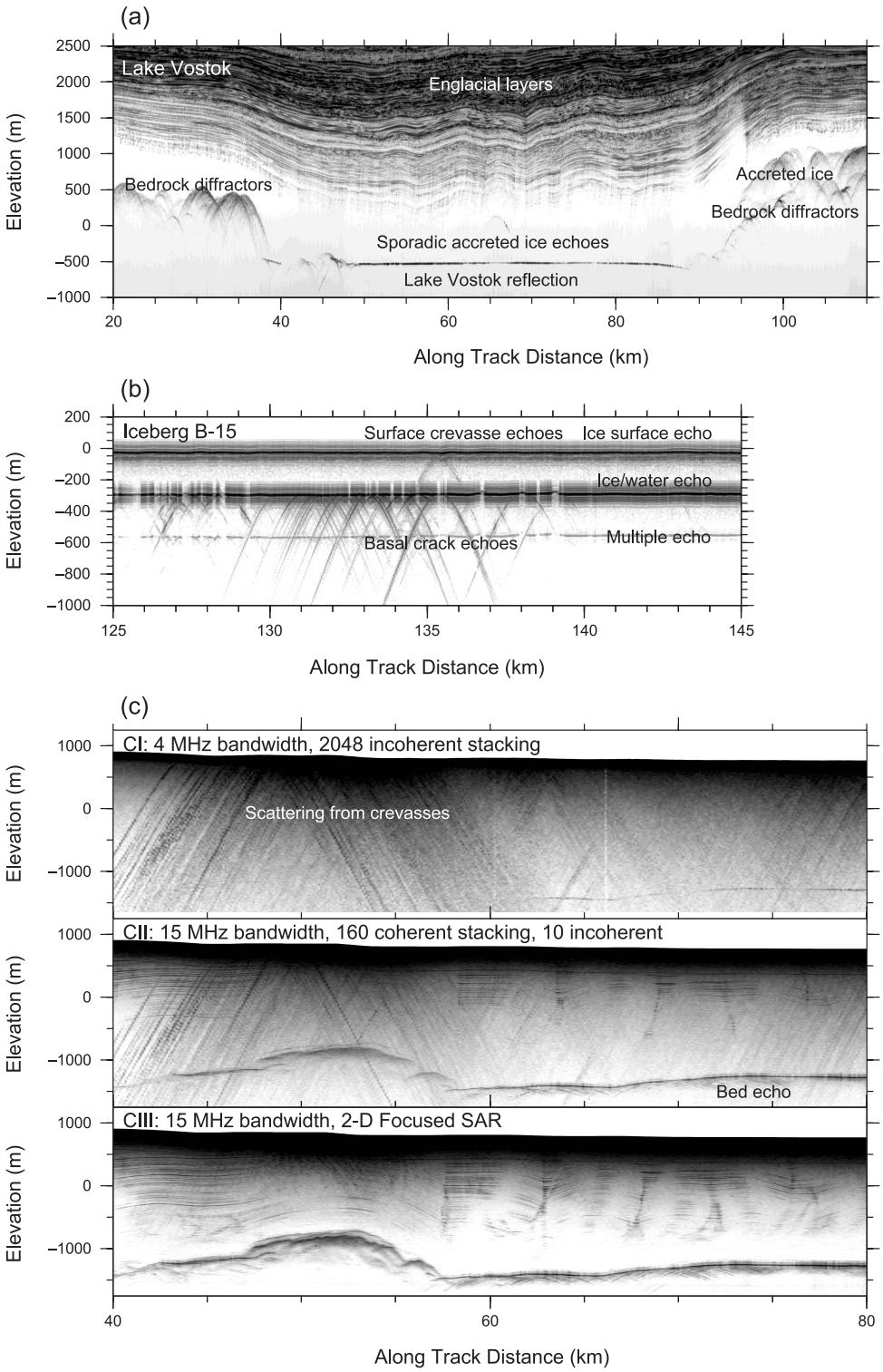

Fig. 3. Three examples of terrestrial radar sounding, all using a 60-MHz radar sounder. **(a)** Example of a radargram from the Lake Vostok airgeophysical survey. The radar is incoherent with 4-MHz bandwidth. The radar data has been converted to absolute magnitudes and logarithmically scaled. **(b)** Example of a radargram from a 15-MHz bandwidth radar across an iceberg (*Peters et al.,* 2007b). These data are incoherently processed. Point corner reflectors (bottom cracks) appear as clearly identifiable hyperbolas as each point is seen by multiple successive pulses. **(c)** Contrasting sounding radars of different bandwidth and processing methods, taken over the onset of Kamb Ice Stream; in CI we show an older, low-bandwidth radar that did not record the phase of waveforms, and thus cannot screen out surface clutter through post-acquisition processing (*Blankenship et al.,* 2001). In CII, we compare a more modern high-bandwidth radar (*Peters et al.,* 2005), with a 3.5-m unfocused aperture length, which reduces some clutter and reveals new bed topography. CIII shows the same data processed using two-dimensional focused SAR and a 2-km aperture length (*Peters et al.,* 2007a). Much more detail in the bed and layers is revealed, while along-track clutter is eliminated.

of the same bandwidth. This enhancement is important, given the –95 dB geometric power loss due to the 330-km-high orbit.

A second method of increasing the signal quality is to increase the pulse repetition frequency (PRF), and add the collected waveforms. The useful PRF is limited by the motion of the radar system with respect to the ground target, and the time delays required to accommodate both the targeted span of ranges and the distance between the radar platform and the target. For a fast moving, distant satellite like the Mars Reconnaissance Orbiter, the pulse repetition frequency is limited to 700 Hz by the pulse travel time (*Seu et al.,* 2007). In the example of the University of Texas' HiCARS radar sounder, mounted on a slow-moving, low-flying aircraft, the PRF used is 6408 Hz (*Peters et al.,* 2005).

Returning signals must be digitized at a rate that correctly samples the returning waveform without aliasing, i.e., at least twice the signal frequency. For VHF frequencies this can be technically challenging. One approach is to use multiple digitizers operating out of phase of one another. As the carrier frequency is often much higher than the bandwidth, a more sophisticated approach is to recognize that much of frequency content of the signal is redundant. Mixing a generated monochromatic waveform back into the signal allows *downconversion* to a manageable frequency range that is only slightly larger than the bandwidth.

3.2. Clutter Reduction and Azimuthal Resolution

The lateral resolution of the system is in part determined by the nature of the target, and the design of the system. For surfaces smooth at the length scale of the carrier wavelength, the resolution will be determined by the *Fresnel zone* (D_F). The Frensel zone is the spot below the radar over which reflected echoes have similar phase, and thus reenforce. As one moves away from the nadir point, the phase of echoes will systematically shift, until destructive interference occurs (see Fig. 2). So far as the radar is concerned, the Frensel zone is illuminated simultaneously. The Fresnel zone for the single layer case can be calculated by

$$D_F = 2\sqrt{\left(r + \frac{\lambda}{4}\right)^2 - r^2} :\sim: 2\sqrt{\frac{r\lambda}{2}}$$

For rougher surfaces, phase coherency will not be preserved. Instead, a weaker echo will be returned from a larger region defined by the transmitted bandwidth of the system. The equation for the single layer *pulse-limited footprint* is

$$D_P = 2\sqrt{\left(r + \frac{c}{BW}\right)^2 - r^2}$$

For smooth horizontal interfaces, the earliest echo will represent the nadir point. However, regions of more complexity (and of interest) will suffer from the indiscriminate wide beams of physical radio antennae. Echoes of the same range but different location overlap. This phenomenon is called *clutter* (see Fig. 2a). To reduce clutter from surface features, the radar system needs to narrow its beam size.

For a simple dipole antenna of length L_t, the half-power beam width in radians (*Campbell,* 2002) is given by

$$\theta_{antenna} = \frac{0.88\lambda}{L_t}$$

The resulting beam pattern will have enhanced gain perpendicular to the dipole, while having nulls aligned parallel to the dipole. It can be seen that the beam width can be reduced, and hence the resolution improved, by decreasing the wavelength to antenna length ratio. For wavelengths able to deeply penetrate ice (ranging from 1 to 300 m), this formula implies a large antenna to obtain focusing. Such antennas are usually technically precluded from free-flying systems.

Because of the broad beam pattern obtained from typical radar antenna, without further processing, targets will be detected in multiple records. Point scatterers are smeared out into hyperboloids as the radar passes the target with changing range (Fig. 2c). Energy from such scatters at the surface can obscure reflections of interest deeper in the ice. To reduce this clutter, the radar beamwidth along-track must be reduced. The motion of the platform allows a means of doing so.

Reducing the angular width of the radar beam, and thus increasing the gain, is done through constructive interference of nadir signals and destructive interference of off-nadir signals. This can either be done physically, by using the real aperture of an antenna, or electronically, by recording waveforms at a high enough sampling rate so as to preserve phase information. Such a radar is known as *coherent*. As the radar platform moves, it can "stack" independent waveforms digitally, a technique known as synthetic aperture radar (SAR). The SAR method, while potentially more powerful than using a real antenna for radar wavelengths, only works in the along-track dimension for a single antenna system.

Unfocused SAR involves coherently adding consecutive waveforms without adjusting their phase (i.e., *Peters et al.,* 2005; *Seu et al.,* 2007). To ensure that only coherently resolved echoes from a contiguous Fresnel zone are being illuminated, the maximum along-track integration distance (the aperture, L) is the same length as the Fresnel zone. The operation is simple enough to be conducted in real time, prior to recording. The result for flat surfaces will be elimination of echoes fore and aft of the nadir spot, and enhancement of the power of the nadir echo that is directly proportional to the number of pulses received over the aperture (see Fig. 2b). The along-track beam width in radians ϕ_x is

$$\phi_x = \frac{\lambda}{2L}$$

A disadvantage to this approach is that echoes from sloping surfaces are canceled out.

With ancillary data regarding platform position and velocity, more sophisticated processing can be performed. Instead of filtering out signals with off-nadir origins, we can use *focused SAR* (*Legarsky et al.,* 2001; *Peters et al.,* 2007a; *Heliere et al.,* 2007) by using the phase history of the returns to establish the target's azimuth in each record (see Fig. 2c). Because of limited bandwidth, the phase of the echo near the nadir will be far more sensitive to basal topography than the apparent range measured from the echo delay. In one-dimensional focused SAR (*Legarsky et al.,* 2001; *Peters et al.,* 2007a; *Heliere et al.,* 2007), a matched filter processor convolves a model for possible phase-azimuth relationships for a given range. However, once the range to a target begins to change significantly, this convolution will fail, limiting the length of the aperture, effectively, to the diameter of the pulse limited footprint. Two-dimensional focused SAR (*Peters et al.,* 2007a) involves a correlation on both phase and range data, allowing much larger apertures to be synthesized, and thus narrower effective beam widths. In theory, the aperture can be as long as the target is in sight of radar, although in practice it is limited by waveform duration, storage capacity for full phase waveforms and significant processing capacity. Longer apertures also allow steeper specular surfaces to be detected, as echos from shallower angles are retrieved (see CIII in Fig. 3c).

To prevent aliasing, waveforms need to be recorded for SAR processing at more than twice the maximum rate of observed phase change (the Doppler bandwidth) (e.g., *Franceschetti and Lanari,* 1999). The Doppler bandwidth implies the minimum data rate required to achieve the maximum resolution of the system. For an airborne system the Doppler bandwidth is calculated as

$$f_{Doppler} = \frac{2v}{\lambda}$$

where v is the platform velocity.

For a spacecraft in a circular orbit around a slowly rotating spherical body, it would be

$$f_{Doppler} = 2\frac{R}{\lambda\sqrt{\frac{(R+h)^3}{GM}}} \quad (2)$$

where R is the radius of the body, h is the height above the surface, G is the universal gravitational constant of 6.673×10^{-11} m^3 kg^1 s^2, and M is the mass of the body. This formula assumes that the antenna beam has little along-track directionality.

3.3. Clutter and the Center Frequency

We have shown that much of the along-track clutter can be removed by using a coherent radar. However, cross-track clutter produced by scattering is difficult to address, especially for orbiting systems. Interpreting sounding radargrams under these conditions requires a good understanding of the scattering processes, as well as being of intrinsic interest (see chapter by Moore et al.). Clutter can be divided into two classes: *random* clutter, which is derived from subresolution, statistically homogenous structures, and *deterministic* clutter, which comes from discrete sources that are resolvable in the radar bandwidth. A second impact of random clutter processes is an attenuation of throughgoing signals, as transmitted energy is scattered away from the receiving antenna.

Random clutter can be separated into three components: quasispecular scattering, diffuse scattering, and volume scattering. In quasispecular scattering, the incoming signal reflects off of facets whose slope variation is small over a resolution bin. Therefore there will be coherent summation of adjacent echoes (similar to the case of SAR focusing above), which imparts a strong directionality on the backscattered echo. For wavelength-scale roughness that has a length scale much smaller than a resolution cell, phase will be uniform in the recorded echoes, and neither constructive or destructive interference will dominate. The backscattered power will be less than the specular return, but the signal will be weakly dependent on across-track angle. *Campbell and Shepard* (2003) point out that for long wavelength systems with high bandwidth, this assumption may break down as the range-defined resolution cells shrink in horizontal size away from nadir.

In the case of volume scattering, point diffractors with dimensions near a wavelength within the sounded medium contribute to the backscatter, again with a low angular dependence. For centimeter-scale wavelengths, this effect can dominate backscatter of icy moons (*Ostro and Shoemaker,* 1990; *Ostro et al.,* 2006; *Wye et al.,* 2007; see chapter by Moore et al.) and even provide apparent reflection coefficients greater than 1, as energy is being returned from a volume instead of a surface.

Resolvable features off nadir introduce deterministic clutter that can complicate the interpretation of subsurface echoes. On the Mars Advanced Radar for Sounding and Ionospheric Studies (MARSIS) (*Picardi et al.,* 2005) in orbit around Mars, a receive-only monopole oriented perpendicular to the main dipole was intended to preferentially detect off-nadir echoes, thus allowing cancellation. Low signal-to-noise precluded use of this antenna (*Plaut et al.,* 2007), and indeed it may not have successfully deployed (*Adams and Mobrem,* 2006). However, MARSIS has demonstrated that, if high-resolution digital elevation models (DEMs) of the surface are available, radar models can be constructed that simulate most relevent surface echoes (*Nouvel et al.,* 2004; *Picardi et al.,* 2005). Comparison of such synthetic radargrams with the real radargram allows true subsurface echoes to be isolated and identified. Conversely, echoes can be picked out of a radargram, and mapped back onto a DEM (*Holt et al.,* 2006).

Most sounder systems cannot distinguish between echoes arriving from the left or right sides of the track. Imaging radar systems [for example, the radars on Magellan (*Saunders et al.,* 1992) and Cassini (*Elachi et al.,* 2005)] resolve this issue by using a high enough frequency so that they

can ensure that the entire beam points to one side of nadir. This approach implicitly assumes that only one interface is observable, which makes them inappropriate for airborne or orbital deep sounding. It has been suggested that the interference patterns between the surface and bed signals can be used to unwrap ice thickness in this geometry (*Jezek et al.,* 2006); however, in this case valuable internal structures must be ignored. Side-looking geometries have been demonstrated for groundbased systems, although significant coverage has not been obtained (*Musil and Doake,* 1987; *Gogineni et al.,* 2007).

Ice-penetrating radar systems have traditionally operated in two bands: HF (3–30 MHz; 10–100 m wavelength in free space) and VHF (30–300 MHz; 1–10 m wavelength in free space). The UHF band (300 MHz to 3 GHz; 0.1–1 m) has typically been restricted to shallow ice sounding (e.g., *Spikes et al.,* 2004), although it is now being investigated for Earth orbital ice sounding (*Jezek et al.,* 2006; *Heliere et al.,* 2007), because of limited ionospheric distortion and regulatory availability. As bandwidth is restricted by the carrier frequency, VHF systems have a superior range and azimuth resolution (tens of meters in ice) to HF systems (hundreds of meters). Random clutter is more of an issue for VHF systems, as by Rayleigh's law for structures much smaller than a wavelength, the scattered power intensity increases by the fourth power of the frequency, and must be considered in planetary radar design. Conversely, the difficulty in fielding antennas with high lateral directionality for HF systems means that deterministic clutter will be unavoidable, especially for orbital systems.

A good example of these tradeoffs comes from recent observations of Mars' ice-rich north polar layered deposits (NPLD) (*Phillips et al.,* 2008). The SHARAD system, operating at 20 MHz with 10 MHz of bandwidth, provides an excellent view of the internal layer structure of the upper portion of the NPLD, but cannot penetrate a rough, dust-rich basal unit; the MARSIS system, operating at either 3, 4, or 5 MHz with 1 MHz of bandwidth, poorly resolves internal layering, but retrieves a strong echo beneath the basal unit. A multifrequency approach will be optimal for orbital radar sounding of Europa's icy shell.

4. RADAR OBSERVATIONS OF THERMAL/COMPOSITIONAL HORIZONS AND STRUCTURES IN EARTH'S ICE SHEETS

The fact that Earth's ice sheets are soundable by radar was discovered accidentally during HF ionospheric observations at the United Kingdom's Halley Antarctic station (*Evans,* 1961), because of destructive interference with the floating ice shelf's basal echo and the failure of UHF aircraft radar altimeters over deep ice (*Waite and Schmidt,* 1962). This property has been subsequently exploited for investigating ice sheet thickness and internal properties (see reviews by *Bingham and Siegert,* 2007; *Dowdeswell and Evans,* 2004). Below we provide an overview of a range of terrestrial targets sounded by radar sounders. The most obvious analog for Europa subsurface targets are subglacial and englacial water bodies and their associated thermal and compositional horizons and structures.

4.1. Flat Subglacial Interfaces

Subglacial lakes in Antarctica were first revealed by their effect on the overlying surface, as the overriding ice flattened through decoupling with the bed, causing landmarks that could be exploited by airborne navigators (*Robin et al.,* 1977). Later airborne surveying revealed that bright continuous basal reflectors with a slope opposing that of the surface (see review by *Siegert,* 2005, and references therein). The most famous example is Lake Vostok (see Fig. 3a).

If the base of the ice is at the pressure melting point, water is present. For a static water-ice interface, the slope at the base of the ice must balance the variation in the the weight of overlying ice, i.e., the lake surface is in hydrostatic equilibrium. This slope criterion can be expressed as

$$\frac{d\left(z_{ice} - h\left(1 - \frac{\rho_{ice}}{\rho_{water}}\right)\right)}{dx} = 0 \qquad (3)$$

where z_{ice} is the ice surface elevation with respect to the geoid, h is the ice thickness, ρ_{ice} is the density of ice, ρ_{water} is the density of water, and x is horizontal distance. When this condition is met, there is no local pressure gradient and the water-ice interface will be stress-free. *Carter et al.* (2007), using collocated airborne laser altimetry and radar-sounding profiles, used this condition as a primary criteria for automatically identifying subglacial lake candidates under East Antarctica's ice sheet. Their classification process for these subglacial water bodies is instructive for understanding potential water discrimination on Europa — bounding any stresses being supported by the overlying ice.

4.2. Attenuation Within the Ice

Carter et al. (2007) used a secondary property of the basal interface to classify subglacial lake candidates: the basal echo strength. The ice-water interface should have a reflection coefficient — the ratio of transmitted into the bed to that reflected — of between –3 and 0 dB (*Peters et al.,* 2005).

The measured echo strength will be much less than this, and needs to be corrected using the radar equation (equation (1)), in order to identify the composition associated with a particular dielectric horizon (*Peters et al.,* 2005; *Neal,* 1979). In addition to the factors listed in equation (1), the attenuation because of the finite permittivity of the ice needs to be addressed. *MacGregor et al.* (2007) present a review of ice absorption in terrestrial ice sheets. Ice absorption in terrestrial ice sheets is primarily a function of the conductivity of the ice, and can be expressed as

$$\alpha \approx 0.912\sigma \text{dBkm}^{-1}$$

where σ is the conductivity in μSm^{-1} (*Evans,* 1965).

TABLE 1. Depth-integrated attenuation rates for Antarctica.

Location	Two-Way Attenuation	Reference
Ronne Ice Shelf	9 ± 1 dB km^{-1}	*Corr et al.* (1993); measured
Interior Ross Ice Shelf	17.3 dB km^{-1}	*Bentley et al.* (1998); measured
Interior Ross Ice Shelf	18 dB km^{-1}	*Peters et al.* (2005); measured
Dome C, East Antarctica	20.2 dB km^{-1}	S. P. Carter, personal communication, 2008
Siple Dome	20.9 ± 5.7 dB km^{-1}	*MacGregor et al.* (2007); calculated
Siple Dome	25.3 ± 1.1 dB km^{-1}	*MacGregor et al.* (2007); measured
Iceberg B15	22.5 dB km^{-1}	*Peters et al.* (2007b); measured
Taylor Glacier	22–32 dB km^{-1}	*Holt et al.* (2006); calculated
George V Ice Shelf	26.8 ± 1.5 dB km^{-1}	*Corr et al.* (1993); measured

In turn, conductivity is mainly controlled by the temperature of the ice and impurity content. The conductivity of ice can be expressed as a series of Arrhenius functions (e.g., *Corr et al.,* 1993)

$$\sigma = \sigma_{ice} e^{\frac{E_{ice}}{k}\left(\frac{1}{T}-\frac{1}{T_r}\right)} + : \mu_{acid} : e^{\frac{E_{H^+}}{k}\left(\frac{1}{T}-\frac{1}{T_r}\right)} \times [\text{acid}] + : \mu_{ssCl^-} : e^{\frac{E_{Cl^-}}{k}\left(\frac{1}{T}-\frac{1}{T_r}\right)} \times [\text{ssCl}^-] + : \mu_{NH_4^-} : e^{\frac{E_{NH_4^-}}{k}\left(\frac{1}{T}-\frac{1}{T_r}\right)} \times [NH_4^-]$$

where σ_{ice} is the conductivity of pure ice; μ_X, E_X, and [X] are the molar conductivity, activation energy, and molar concentration in μMol of ionic component X, respectively; T is the ice temperature in Kelvin, and T_r is a reference temperature of 251 K; and k is Boltzmann's constant. The major impurities important for meteoric ice (ice precipitated from the atmosphere) are acids and sea-salt-derived chlorides, with ammonia being important in the northern hemisphere.

At Siple Dome, Antarctica, where temperature and ionic concentrations are available from an ice core, *MacGregor et al.* (2007) found that the contribution from pure ice dominated loss for ice temperatures above 30°C (243 K); this temperature will be highly dependent on ionic concentrations. Measured and calculated rates of ice attenuation at various locations in the Antarctic Ice Sheet can be found in Table 1. When comparing these values to those calculated for Europa in the next section, one should bear in mind that while the base of the ice is at the pressure melting point, the surface temperature of the ice sheet (210 to 240 K) is dramatically warmer than that of Europa (~100 K).

For Earth's ice sheets, lateral flow of ice, the potential for basal melting, and ice dynamic timescales on the order of major climate variations mean that the internal temperature structure of the ice remains one of the great problems in glaciology. Given the implications of temperature for the radar equation, the search for subsurface water would benefit from a search for the absolute value of the basal reflection coefficient. In fact, it has been common to utilize relative variations in basal echo strength to identify free water (e.g., *Gades et al.,* 2000; *Catania et al.,* 2003) or fix the attenuation rate using a point reference where the basal reflection coefficient is believed to be known (*Shabtaie and Bentley,* 1987; *Bentley et al.,* 1998; *Peters et al.,* 2005).

Carter et al. (2007) used both methods to classify subglacial lakes, combining impurity estimates from distant ice cores and one-dimensional models of ice sheet thermal structure to derive loss values over lake candidates. Lake candidates that were both 2 dB more reflective than their surroundings, and had an absolute reflection coefficient above –10 dB, were classified as definite lakes; if a candidate failed the absolute reflection coefficient critera, it was classified as a "dim" lake. Because these dim lakes were in clusters and in hydrostatic equilibrium it was recognized that the attenuation model overestimated the amount of absorption over these candidates, with implications for thermal history and impurity fluxes in the overlying ice. A similar approach will be necessary for any water search at Europa, although both impurity flux and thermal evolution will need to be hypothesized.

Vertical variations in the dielectric properties of ice lead to radar layering. Englacial radar layers in ice have been long identified in studies of terrestrial ice sheets (see *Dowdeswell and Evans,* 2004) (Fig. 3a). These layers corresponding to the chemical, density, or crystal fabric stratigraphy of the ice. On Earth at 1–100 MHz radar-sounding frequencies, chemical variations dominate, with the source of the layers ultimately tied to acidic aerosols from volcanic eruptions, a hypothesis verified through connecting layers to ice cores (e.g., *Jacobel and Welch,* 2006). While radar layers due to particle inclusions are less common on Earth, they have been identified in some locations (*Corr and Vaughan,* 2008).

4.3. Accreted Ice at Ice Shelves and Lakes

While the vast majority of terrestrial ice is meteoric in origin, some originates from liquid reservoirs, with different chemistry. An example is found in West Antarctica's central Ronne Ice Shelf. The results of analog airborne radar sounding from 1969 appeared to show that much of this ice shelf was anomalously thin and had echo strengths much lower

than would be expected for a smooth ice water interface (*Robin et al.,* 1983); it was hypothesized that unusual ice dynamics were locally thinning the ice shelf, with the low echo strengths being explained by saline, lossy basal ice, as observed in the Ross Ice Shelf (*Neal,* 1979). A more advanced radar sounder was flown over the ice shelf in 1983–1984 (*Thyssen,* 1998), and found that the basal echo split at the edges of the "thinned" area, with the deeper layer being eventually lost. By applying the isostatic criterion (cf. equation (3))

$$z_{ice} - h\left(1 - \frac{\rho_{ice}}{\rho_{water}}\right) = 0 \qquad (4)$$

it was found that up to 400 m of the ice shelf was composed of a discrete package of lossy ice, a result confirmed by boreholes through the ice (*Engelhardt and Determann,* 1987). This remarkable result was due to the oceanography of a sloping ice shelf. High pressures depress the melting point of water ice; thus, very deep portions of an ice shelf will melt. Being fresher than its surroundings, the melt water will rise up the ice shelf front to regions of lower pressure, where it will promptly recrystallize. As the new crystals are lighter than water, they will settle against the overlying ice shelf, while the rising melt water sucks in more warm deep water against the ice shelf. These phenomena are termed "ice pumps" (*Lewis and Perkin,* 1986).

The result is a slowly compacting layer of ice crystals immersed in very saline, electrically conductive brines termed *marine ice* (see section 2.1) (*Moore et al.,* 1994). Typical attenuation rates for marine ice at the pressure melting point range from 140 to 300 dB km^{1} (*Blindow,* 1994). However, the lower interface of an actively accreting ice shelf may also be gradational at radar wavelengths (*Engelhardt and Determann,* 1987), preventing a sharp reflective interface. Timescales available for settling in an ice shelf environment, however, are short; ice shelf spreading rates are on the order of a kilometer per year, so most marine-ice deposits are destroyed within a few centuries, leaving little time for trapped brines to migrate out of the ice. Given ice thickness and surface elevation with respect to the geoid, deviations from equation (4) can be used to map out the distribution of basal accretion (*Fricker et al.,* 2001), a tool that may be useful for Europa.

Accretion is also observed at subglacial lakes. At Lake Vostok (Fig. 3a), enough of a pressure melting point gradient exists to drive an ice pump, and thus accretion at one end of the lake. Fortuitously, we have samples of this ice through the Vostok core (*Souchez et al.,* 2004, 2003). In this case the opposite attenuation properties are seen; conductivity decreases in the accreted section, because of a near complete loss of acids (*De Angelis et al.,* 2004). The interface between accreted and meteoric ice is visible in radargrams (*Oliason and Falola,* 2001; *Bell et al.,* 2002) as a low-amplitude horizon above the main lake reflector. However, lake surface reflection coefficients are not strongly perturbed by the accretion layer (*Carter et al.,* 2007). This lack of impact on the loss profile of the ice column is primarily due to the low salinity of the layer; however, it may be a function of the 25,000 years needed to advect the accreted ice across the lake surface, as residual liquid between crystals drains back into the lake.

4.4. Vertical Structures

Tension fractures generally dominate the grounded ice sheet surface where there are large gradients in ice velocity, whereas tension fractures dominate both the surface and base of the ice where grounded ice sheets (or ice streams) transition to floating ice shelves. The process that controls the distribution of these fractures is the balance between the spatial strain rate gradient and the ability to accommodate these strain rates through annealing (which is a function of temperature). Similarly, pervasive and nearly chaotic shear fractures characterize the lateral boundaries of the ice streams over regions that are many times the ice thickness in width. The ice streaming process that controls the position and width of these zones is dominated by stress concentrations at the boundaries of gravity-driven slab flow.

Vertical structures cannot be directly imaged using a nadir-pointed sounding system. However, scattering points at edges can be detected, and where a vertical plane intersects a horizontal surface, a corner reflector geometry will occur when the platform track is oriented perpendicular to the vertical surface. This property can be exploited to examine both the composition and size of a vertical structure.

The giant Antarctic iceberg B-15 was surveyed in December 2000 and December 2004 (Fig. 3b). The data were acquired using the University of Texas at Austin's high-bandwidth coherent HiCARS system in 2001 (*Peters et al.,* 2005). On this occasion, the data was analyzed without any SAR processing in order to look at basal diffractors with a range of look angles and identify corner reflectors that we reinterpreted as the lower edges of basal cracks (*Peters et al.,* 2007b). The classification includes major crevasses filled with seawater and incipient or freezing crevasses that are either small with seawater or larger with marine-ice accretion. The large water-filled crevasses likely exhibit varying amounts of marine-ice accretion with moderate brine inclusions. Crevasse height estimates were obtained under the assumption that all crevasses have interfaces similar to known water-filled crevasses or iceberg edges. These statistics are indicative of the basal dynamics of the seawater/iceberg interface.

4.5. Volume Scattering

Volume scattering has presented a challenge to sounding terrestrial ice. *Peters et al.* (2005) presented a map of derived reflection coefficients for the lower reaches of two West Antarctic ice streams, Whillans Ice Stream and Kamb Ice Stream (formerly "Ice Stream C"). This map (Fig. 4) was derived from airborne data collected in 1987 (*Bentley*

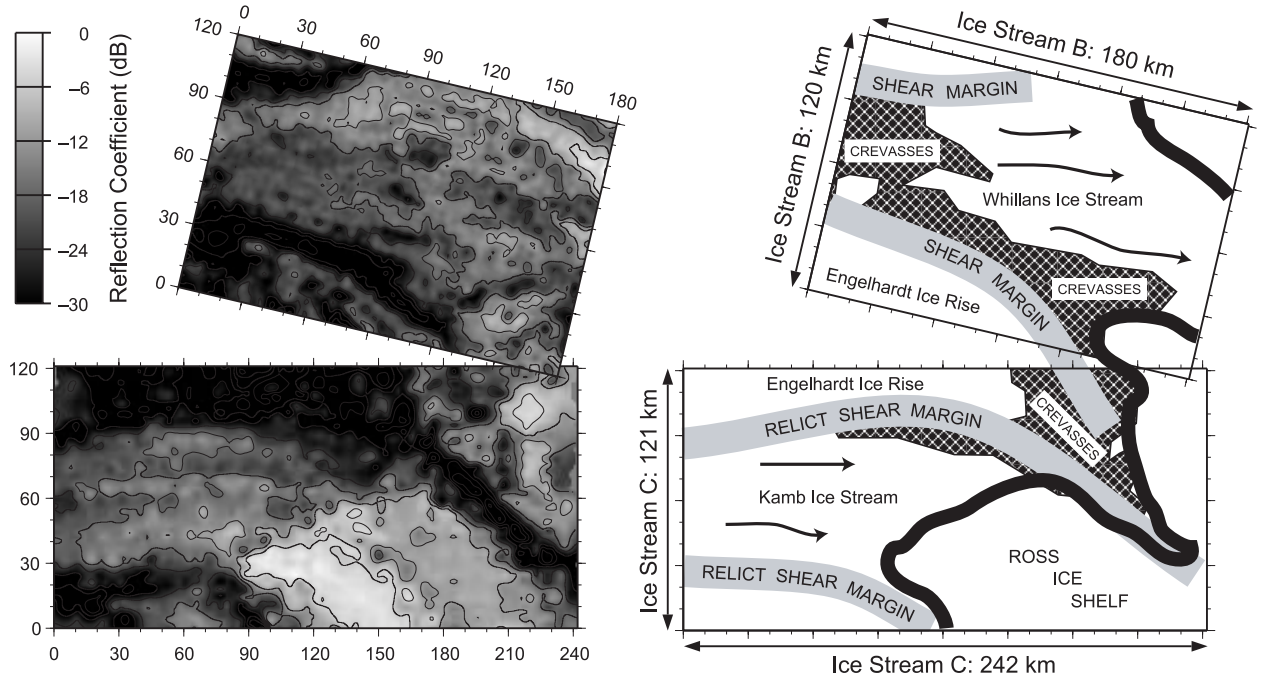

Fig. 4. Map of basal reflections and corresponding sketch map from coherent radar sounding of West Antarctic ice streams (*Peters et al.,* 2005). White regions (high reflection coefficient) correspond with floating ice; narrow dark lanes (low reflection coefficient) correspond to shear margins.

et al., 1988, 1998). The radar sounder was a coherent system with a wavelength of 6 m using a unfocused synthetic aperture of 40 m, resulting in an along-track spot size of ~40 m at the ice surface.

Although seawater is easily identified in these basal reflection maps, in the shear margins of the ice streams the apparent basal reflection coefficients abruptly drop by 20 dB. Pervasive surface crevasses, several meters wide, line the ice streams and effectively attenuate throughgoing signals. The effect of this was demonstrated when the ICESAT laser altimetry experiment, monitoring surface elevation changes, detected an extensive subglacial water system (*Fricker et al.,* 2007) beneath the northern margin of Whillans Ice Stream with a predicted reflection 36 dB higher than observed in these radargrams.

Focused SAR, unavailable for the 1987 radar data, can improve on this performance by effective allowing more independent "looks" at a single bed target. *Peters et al.* (2007a) demonstrated this algorithm on the upstream portions of Kamb Ice Stream. Coherent waveforms were recorded with a PRF of 6400 Hz that was coherently stacked to 400 Hz (well above the Doppler bandwidth of 28 Hz) and processed with both an unfocused aperture of 70 m and a two-dimensional focused aperture of ~1500 m. The result, shown in Fig. 3c, is an astonishing increase in resolvable structure (and improved resolution) as well as a significant increase in the basal echo strength under active shear margins for the focused SAR case. These techniques form the benchmark for approaches to sounding the subsurface of Europa's icy shell.

Because water pockets exist at the melting point of ice, volume scattering is dominant in temperate terrestrial ice caps and glaciers. For these bodies, pervasive englacial water pockets act as a cloud of diffractors greatly increasing the apparent scattering cross section (*Bamber,* 1988). These pockets also merge to form englacial conduits within the ice (*Bamber,* 1987), and freeze to form ice lenses within the more porous snow column (*Paterson,* 1994; *Pälli et al.,* 2003). Because of these characteristics, temperate (and polythermal glaciers) will be important Earth analogs for sounding hypothesized melt-rich targets on Europa.

5. A RADAR-SOUNDING APPROACH FOR EUROPA

As discussed previously, we consider multiple models to represent ice growth mechanisms that may be present on Europa (*Blankenship et al.,* 1999; *Moore,* 2000). The first of these is a europan crust dominated by marine processes (Fig. 5a) with slow accretion (freezing) or ablation (melting) on the lower side of the icy crust with temperature gradients that are primarily a function of ice thickness (*Squyres et al.,* 1983). A second possible mechanism is the very rapid freezing of ocean water in the linear fracture zones caused by tidal/tectonic processes where large temperature gradients will be present. This process could lead to ice with properties similar to sea ice. This tidal/tectonic model (Fig. 5b) (*Greenberg et al.,* 2002) could represent an oceanic imprint on a primordial europan crust that had been well below the melting point throughout its history, or could

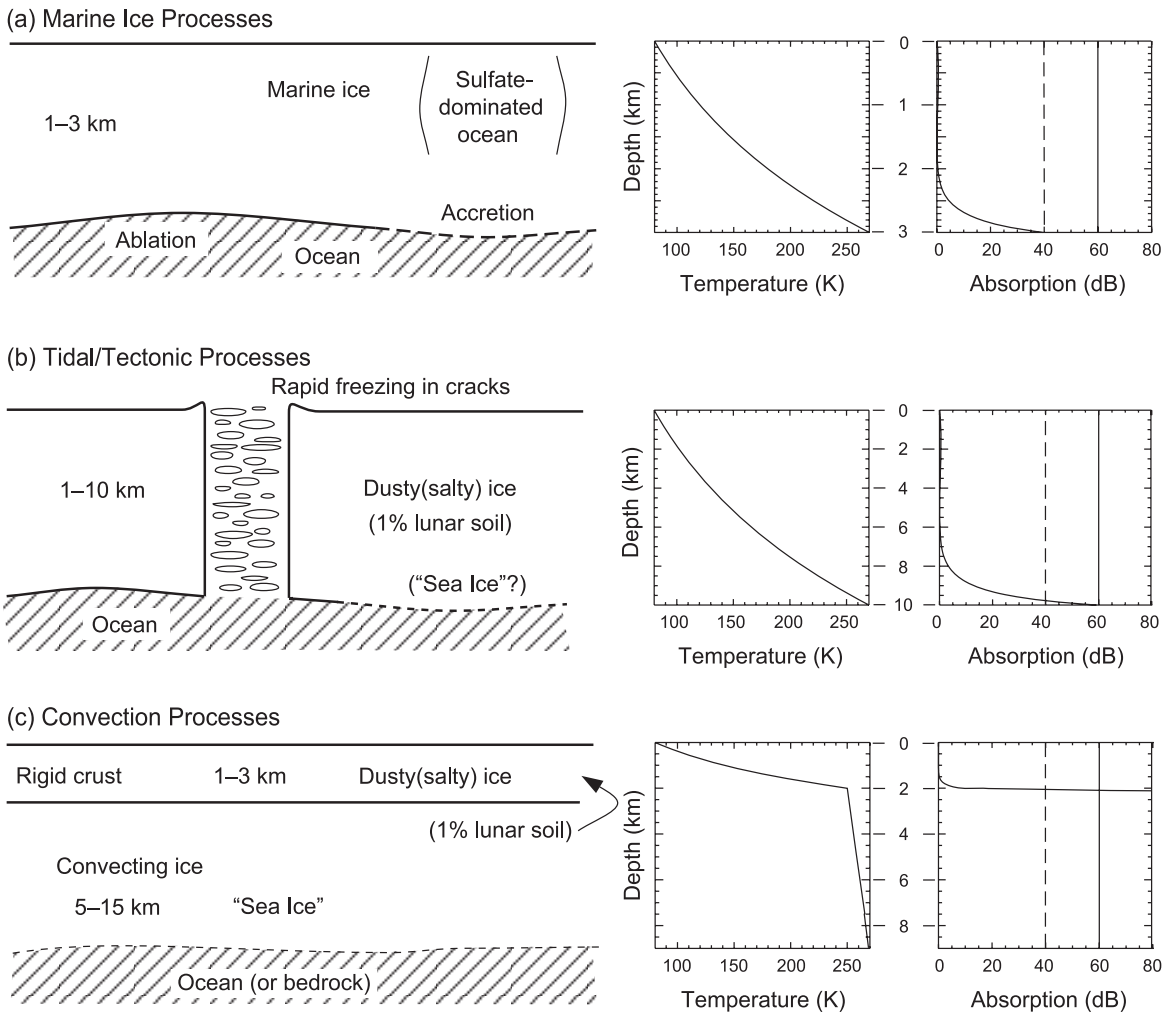

Fig. 5. Schematic diagrams of three ice formation processes that may occur on Europa with expected temperature and radar absorption vs. depth for each assuming a "midlatitude" surface temperature of 80 K (*Blankenship et al.,* 1999). The properties of the component ices and ocean are given in Table 2. **(a)** Model of ice formation similar to that for marine ice on Earth (potentially applicable to Europa's chaotic terrains) with parts of the base subject to melting (ablation) and others to slow freezing (accretion) of frazil ice crystals. **(b)** Ice formation via extrusion into cracks or fissures with rapid freezing (potentially applicable to Europa's ridged terrains). **(c)** Convection scenario with a cold rigid crust underlain by thicker isothermal convecting ice. The dashed and solid lines in the rightmost charts represent approximate system dynamic range for sub- and antijovian Europa sounding with a high-frequency (50 MHz), low-bandwidth (0.85 MHz), and low-power (20 W peak) system.

represent the ice formed entirely by ocean water injected in cracks and then spread over much of the crust by tidally driven tectonic processes. In addition to these two processes, *Pappalardo et al.* (1998) used evidence from Galileo imagery to support the idea of convection in an isothermal layer under a rigid ice crust up to a few kilometers thick that is thermally conducting (Fig. 5c). This convecting ice model could be dominated by ice very similar to that for the tidal/tectonic model although subject to a dramatically different thermal regime.

5.1. Absorption in Europa's Crust

A comprehensive model for electromagnetic absorption in Europa's icy crust was presented by *Moore* (2000). He noted that the species of impurity known to have non-negligible solubility in ice are NH_4^+, H^+, F^-, and Cl^- (*Gross et al.,* 1978) and presented arguments for the dominance of Cl^- in europan ice formation. He then used an activation energy for Cl^- of 0.19 eV (18.4 kJ/mol), measured for marine and meteoric ice on Earth over a wide range of concentrations and at temperatures down to 210 K (*Moore et al.,* 1992), to estimate the absorption of ice derived from a europan ocean with a range of salinities.

Moore (2000) also noted that for impurity concentrations in the ice above a species-dependent solubility limit, the species must be present outside the crystal structure as a liquid or separate salt phase and that radar losses can also come from interfacial polarizations and scattering that occurs whenever the radar waves encounter these mixtures of

TABLE 2. Radar absorption (α) for various ice types and temperatures in Europa's icy shell.

Ice Type	Impurity Content	α(dB m^{-1})	I (dB km^{-1})	II (dB km^{-1})	Notes
Pure ice	Nil	0.0045	1.4–2.4	0.2–0.3	*Glen and Paren* (1975)
Marine-ice (Cl^- Europa)	3.5‰ chlorinity	0.0016	4–7	1.6–2.8	Scaled from Earth; $k_{MI} = 7 \times 10^{-4}$
Marine-ice (SO_4^{-2} Europa)	10‰ chlorinity	0.037	9–16	4–7	*Kargel* (1991) $k_{MI} = 7 \times 10^{-4}$
Dusty/salty ice	1% lunar soil	0.008	5–6	3.6–4.1	*Chyba et al.* (1998) recalculated
Dusty/salty ice	10% lunar soil	0.01	8–9	6–7	*Chyba et al.* (1998) recalculated
Dusty/salty ice	50% lunar soil	0.021	30–33	28–31	*Chyba et al.* (1998) recalculated
Marine-ice (Ronne Ice Shelf)	0.025 chlorinity ice (≈35 ocean)	0.15	36–61	18–31	*Moore et al.* (1994)
Sea ice (Baltic Sea)	≈3 chlorinity ocean	0.85 (at 270 K)	50–85	16–27	*Moore* (2000)

Column I is for a thermally conductive shell with a surface temperature of 50–100 K and its base at the pressure melting point, i.e., over water (≈270 K). Column II is for a thermally conductive shell over "ductile" ice at 250 K. Ice type and impurity content is explained in the text. From *Moore* (2000).

insoluble impurities. Examples of these mixtures were dusty or salty ice (*Chyba et al.,* 1998) and sea ice, where millimeter-scale brine pockets are trapped in the ice by rapid freezing. Because of the large difference in dielectric constant between liquid brine and ice [typical dielectric constants of 86 and 3.2, respectively (*Moore et al.,* 1992)], sea ice is characterized by very large absorption at radar frequencies.

Table 2 reproduces *Moore*'s (2000) estimates of the absorption at radar-sounding frequencies for a range of ices consistent with the europan ice formation processes presented in Fig. 5. Endmembers of the table are pure ice with the conductivity and activation energy given by *Glen and Paren* (1975) and sea ice formed in the relatively low salinity (3‰, parts per thousand) Bay of Bothnia in the Baltic Sea where ice salinities are about 0.5 to ~1‰ and brine pockets are common (*Weeks et al.,* 1990).

Moore's (2000) preferred model for marine-ice formation was based on a straightforward model of the geochemical evolution of Europa (*Kargel,* 1991), which predicts the icy crust to be largely dominated by sulfate salts, mainly $MgSO_4$ and Na_2SO_4, noting that there could also be about 1% by weight Cl, mainly as NaCl and $MgCl_2$. *McKinnon and Zolensky* (2003) have critiqued this view of Europa's geochemistry, using revised meteorite chemistries to suggest a subsaturation concentration of oxidized sulfate in Europa's ocean, and thus a very minor component of Europa's crust; however, this debate has a small impact on our assessment of loss. *Moore*'s (2000) calculation of absorption for the marine-ice models in Table 2 also required an estimate of the distribution coefficient, k, for the Cl^- concentration in ice relative to that in the liquid it is grown in. Table 2 uses a distribution coefficient for marine ice, $k_{MI} = 7 \times 10^4$ (*Moore et al.,* 1994), that is derived from measurements on samples formed under accretion rates observed for the previously described Ronne Ice Shelf in Antarctica.

As an unlikely endmember for marine-ice processes, *Moore et al.* (1994) calculated the absorption losses for the marine ice of the Ronne Ice Shelf using experimental values of conductivity that are well known over the temperature range 200 to 273 K. For marine ice formed by a chloride-dominated europan ocean, *Moore* (2000) used a direct comparison to Earth. Given that the ocean volume to crust ratio for Europa and Earth are about the same, and that the land surface of Earth is about 10 times that of Europa, a simplistic estimate for europan ocean chlorinity is about one-tenth that of Earth's oceans or about 3.5‰. This is consistent with more-detailed geochemical models (*Zolotov and Shock,* 2001) that predict chlorinities ranging from 9.3 to 0.055‰, and with analysis of Galileo magnetometer data that allows for comparatively low salinity for Europa's ocean (*Hand and Chyba,* 2007).

For a sulfate-dominated europan ocean, *Moore* (2000) noted that sulfate ions are not soluble in ice to any significant degree and experiments on ice formed naturally on Earth (and in laboratories) show that SO_4^{2-} seems to play no role in electrical conduction (*Gross et al.,* 1978). He also noted that the permittivity of these solid salts would be similar to that for rock, so the tidal/tectonic processes of Fig. 5b assumed dusty (salty) ice derived from *Chyba et al.* (1998). The 1% soil mixture of *Chyba et al.* (1998) was used as an acceptable representation of the absorption of a sulfate-dominated icy crust on Europa that is being generated and modified by either tidal-tectonic or convection processes.

Given the ice formation processes of Fig. 5, Table 2 also reproduces *Moore*'s (2000) calculated radar absorption averaged over the total ice thickness for a range of possible europan ice. Figure 5 presents the calculated temperature and absorption as a function of depth [T(z) and α(z), respectively] for these ice-formation processes given T_S, the surface temperature, and T_b, the temperature at the base of the thermally conducting layer: The surface temperatures on Europa were assumed to range from 50 to 100 K. For the marine-ice and tidal/tectonic processes of Fig. 5b, T_b was assumed to be close to 270 K for reasonable ice thicknesses.

In the case of convecting processes, where a cold brittle outer crust is underlain by warmer convecting ice that is

nearly isothermal at perhaps 235–260 K, *Moore* (2000) chose the the value of T_b for the conducting layer to be the temperature of the isothermal layer. Interestingly, because the radar absorption is governed by the exponential dependence on temperatures, he showed that an average two-way absorption (per kilometer) that is independent of total ice thickness can be found for a given surface temperature. Table 2 reproduces *Moore*'s (2000) averaged two-way radar absorption per kilometer of total ice thickness for two conducting models: one with T_b = 270 K corresponding to marine ice or tidal/tectonic ice in contact with an ocean, and one with T_b = 250 K corresponding to the base of the cold brittle shell of the "convection" model. The range of absorption for each of the conducting models in Table 2 corresponds to a range of surface temperatures (50–100 K) on Europa.

5.2. Noise Environment

Any radar sounding of Europa's icy shell will be constrained by the radio noise environment, which is impacted by two main sources: galactic background noise and emissions from Jupiter's extensive ionosphere. It has been known since the 1950s that Jupiter is a major source of HF radio noise (*Burke and Franklin,* 1955). It was subsequently found that a substantial portion of this decametric emission (DAM) occurs when the electron flux tube connecting Io to Jupiter is dragged over certain longitudes of Jupiter's polar regions (*Bigg,* 1964). The result is an episodic energetic beam emitting at frequencies between 8 MHz and 40 MHz (*Zarka,* 2004). Other, less-well-understood sources, linked to specific sites within Jupiter's magnetic field and tied to Jupiter's rotation, emit narrow episodic beams between 2 and 40 MHz (*Zarka,* 2004). These cyclotron masers abruptly cut out at 40 MHz, and the VHF background is dominated by continuous synchrotron emissions from Jupiter's radiation belts that are ~50–60 dB lower in intensity (Fig. 6).

Observations during Galileo's E12 encounter, which came within 201 km of Europa's antijovian hemisphere, indicate that Europa does screen out RF noise for a portion of the antijovian hemisphere (*Kurth et al.,* 2001). However, given the 100–200-km height of an orbiting spacecraft over Europa, Jupiter's large angular size as seen from Europa, and Europa's synchronous rotation, observations of up to three-quarters of Europa's shell could be exposed to this episodic HF noise, especially the polar regions. The power intensity of episodic DAM events at Europa, scaled from *Zarka et al.* (2004), would be ~–28 dBm at 5 MHz and 1 MHz bandwidth; at 50 MHz and 1 MHz bandwidth, the power intensity is –99 dBm because of continuous synchrotron emissions observed around subjovian Europa (*Zarka,* 2004) and –123 dBm because of the galactic background (*Cane,* 1979), which could be observed from about half of Europa's antijovian hemisphere.

Given the tight beams of the DAM emission, the impact of these events on HF radar observations would vary regularly as Io and Jupiter rotate with respect to Europa. Comparison with Cassini Radar and Plasma Wave Science (RPWS) instrument flyby data (e.g., *Zarka et al.,* 2004) suggest that at 5 MHz, at least 55% of unocculted radar observations would escape interference from DAM emissions. Lastly, the well-shielded portion of Europa's farside includes many important targets for exploration, such as Argadnel Regio and Thrace.

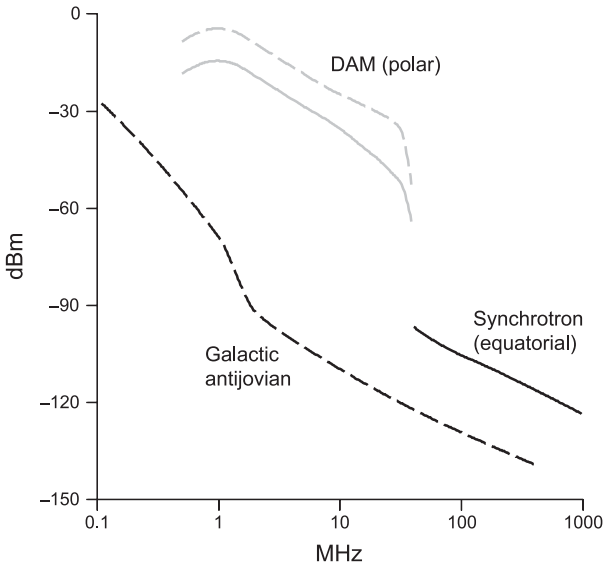

Fig. 6. Radio noise power at Europa, for a 1-MHz bandwidth receiver and an omnidirectional antenna. The data for the subjovian hemisphere (showing episodic polar DAM and continuous equatorial synchrotron noise) is compiled from Cassini and terrestrial observations (*Zarka,* 2004), while the calculation of galactic noise, appropriate for the antijovian region, comes from *Dulk et al.* (2001). The peak (dotted) and typical (solid) intensities of DAM events are shown. The large drop in jovian noise above 40 MHz is very apparent.

5.3. Volume Scattering

At UHF frequencies, acquired by Earth-based radar, the radar cross-section from Europa exceeds unity, suggesting extensive internal scattering (*Ostro and Shoemaker,* 1990); however, this return decreases significantly as the wavelength increases (*Black et al.,* 2001). This suggests that low-frequency returns from Europa may be due to surface scattering mechanisms similar to those operating from Earth's icy surfaces.

Eluszkiewicz (2004) performed a worse-case analysis for volume scatterering, examining the case of a regolith with quarter-wavelength-sized cavities [which, for the 50-MHz frequency favored in some studies (*Chyba et al.,* 1998; *Blankenship et al.,* 1999) for Europa sounding, corresponds to ~1 m). *Eluszkiewicz* (2004) found that a 5% porosity regolith with such cavities could have a two-way attenuation of 113 dB.

Lee et al. (2005) used analogy to terrestrial ice to constrain a porosity for the regolith, and suggest a typical pore

size of the centimeter scale. In this case, HF and VHF radar would not be strongly affected.

5.4. Surface Scattering

The ice at Europa's surface is much colder and stiffer that in Earth's ice sheets, and is in a lower gravity field. The results are that at small scales the surface of Europa is much rougher that that of a typical ice sheet. Combined with the wide beam spot implied by the 50–200-km-high orbit of a Europa sounding mission, surface scattering could be significant. Working to mitigate the effect of this clutter is the low surface reflectivity of water ice (ranging from –11 to –26 dB for a porous regolith), and the fact that the power returned by incoherent clutter drops with a $\frac{1}{r^4}$ spreading loss vs. $\frac{1}{r^2}$ for smooth nadir targets.

In order to predict the nature of scattering we need to know the topography of the surface of Europa. Neither the Voyager or Galileo spacecraft carried explicit altimetry instruments; therefore, the best available data for the large-scale surface characteristics of Jupiter's moons is obtained by using combined stereo and photoclinometric DEMs obtained by using Galileo imagery (e.g., *Schenk and Pappalardo,* 2004; *Giese et al.,* 1998). Because of the failure of Galileo's high-gain antenna, high-resolution stereo coverage is limited. Some early work on analyzing the small-scale topographic spectrum of Europa relevant to radar studies is reported in *Blankenship et al.* (1999), *Schenk* (2005), and *Nimmo and Schenk* (2008).

To sample a variety of terrain types, *Blankenship et al.* (1999) examined DEMs generated for Pwyll crater (300 m to 30 km resolution); the "Wedges" region, Argadnel Regio (100 m); and the Conamara Chaos region (20 m to 3 km). They found that the slope distribution at measurable length scales was consistent with a power law distribution. At Pwyll crater, the slope spectrum was consistent with a self-affine Brownian distribution, implying relatively rough slopes at small scales [RMS slope of ~45° at 1 m; see *Shepard et al.* (2001) for an explanation]; however, at Pwyll crater the minimum horizontal resolution was still much larger than candidate sounding wavelengths. Later work by *Schenk* (2005) and *Nimmo and Schenk* (2008) appear to show that at shorter length scales relevant to radar, the power law is closer to a true fractal for many terrains, implying lower small-scale roughness (RMS slopes of ~11°), which would be "smooth" by many radar criteria. Therefore, only geometric optics scattering, which assumes smooth surfaces at a wavelength scale, will be described further.

Using the slope distributions for the Pwyll region, *Blankenship et al.* (1999) predicted a geometrical optics contribution that decreases from about –10 dB to –20 dB as the incident angle varies from 0° to about 20° (for a 200-km-high orbit, this clutter would overlap subsurface echoes ~20 km below the surface). For incident angles greater than 20°, the geometric optics cross section remains roughly constant at about –20 dB for incident angles smaller than 45°. Modeling the scattering from any europan ice/ocean interface remains problematic because the geometry of any presumed interface is uncertain.

5.5. Sounding Europa's Crust

The radar sounding required to search for any ice-ocean interface on Europa and test first-order predictions of ice-ocean exchange by marine and convective processes must have a very high total sensitivity and multikilometer or better horizontal resolution. For the limited region around the antijovian point, an HF system styled on MARSIS or SHARAD may fulfill this requirement. A 5-MHz system with 1 MHz of bandwidth orbiting 200 km above Europa would have an in-ice vertical resolution of 85 m, with horizontal resolutions at the surface ranging from 20 km (pulse-limited) to ~270 m (one-dimensional focused SAR).

To search for shallower subsurface water, a SHARAD-type system (20 MHz bandwidth and 10 MHz bandwidth) would have theoretical vertical resolutions of 8 m, and horizontal resolutions at the surface ranging from 4.9 km (pulse-limited) to ~153 m (one-dimensional focused SAR) at an orbital height of 100 km. However, the severe but episodic RF noise environment for the other three-quarters of Europa's surface could be an operational challenge for any global mapping program using the HF band.

A 50-MHz system with 10-MHz bandwidth would have horizontal resolutions at the surface down to 62 m (one-dimensional focused SAR) at 100 km height. Such length scales are near those required to test hypotheses concerning shallow europan tectonics and impact processes as well as to characterize shallow subsurface water. While Jupiter's synchrotron radiation remains problematic in the VHF band, a 50-MHz system has a greater probability of global success for targets in the top few kilometers. Ten-megahertz bandwidth waveforms would require greater than 20 MHz sampling, a rate that would likely fill data buffers too quickly to characterize a crust of several tens of kilometers in thickness. Theoretically, two-dimensional focused SAR incorporating 1 μs of range data for every resolution cell could resolve structures as small as a few tens of meters; however, the processing requirements are high, and probably too stringent for continuous onboard use. The Doppler bandwidth from equation (2) for such a system is 900 Hz; current downlink technology preclude returning radar records at this rate. High-rate data recorded over local carefully selected targets and later returned to Earth for deeper processing represents a solution to this problem.

A multifrequency system may be the best approach for fully investigating Europa — comprising a high-bandwidth system for shallow crustal studies, and a low-bandwidth, deep-penetration system, with a low enough information density to record over the full depth of the crust. The results of the deep penetration study will be determined in large part by the absorption profile of Europa's crust.

Figure 5 shows the estimated two-way absorption vs. depth for the three proposed ice formation processes on Europa (*Blankenship et al.,* 1999; *Moore,* 2000), and Fig. 7

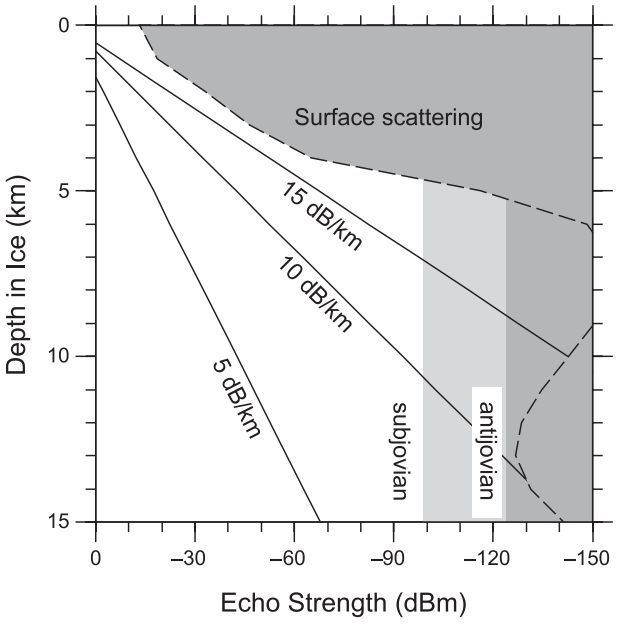

Fig. 7. System performance for a nominal 50-MHz, 0.85-MHz bandwidth Europa radar sounder derived from *Blankenship et al.* (1999) in the context of a Gaussian scattering model (*Peake and Barrick,* 1967) for Europa's surface (dashed lines), and a directional antenna beam pattern. Signal strength is increased by 53 dB through SAR processing and pulse compression. The strength of the return from a specular ice/ocean interface is presented as solid lines with differing ice absorption values (see Table 2). RF noise limits for each side of Europa, derived from Fig. 6, are also presented.

shows the modeled strength of the return from an ice/ocean interface for these processes (*Blankenship et al.,* 1999) for a high-frequency (50 MHz), low-bandwidth (0.85 MHz) system. For both the marine-ice and tidal-tectonic processes (i.e., T_b = 270 K), the ability to characterize any ice/ocean interface or internal layering can be inferred directly from these plots. Recalling that a smooth ice-ocean interface would give negligible reflection losses, Fig. 5 shows that the total absorption is less than a nominal instrumental dynamic range of 60 dB over the full range of total ice thicknesses estimated for both marine and tidal/tectonic ice formation processes on antijovian Europa at 50 MHz. This is also the case for the rougher ice/ocean interface assumed in Fig. 7. In addition, Fig. 7 shows that the range of total ice thickness soundable on subjovian Europa is reduced by about one-third (to a little over 2 km for marine ice and 6 km for tidal/tectonic ice formation processes) compared with antijovian sounding.

For the "convection" processes of Fig. 5, the deeper warm layer is likely to contain brine pockets as the ice temperature will be above the eutectic point of some chloride salts. Because of this, absorption will become very high (similar to the sea ice of the Baltic Sea or even higher; Table 2) and radio waves will be unable to penetrate the convecting ice to any subsurface ocean. If the boundary is reasonably sharp, there will be a radar reflection from it because of the change in dielectric impedance. The magnitude of the reflection will depend on the brine content in the ice and its spatial distribution.

A relevant example on Earth is the reflection coefficient observed at the boundary between cold-dry and temperate-wet glacier ice with an essentially uniform distribution of water pockets, as seen in the Arctic's polythermal glaciers, typically about 20 dB (*Bamber,* 1987). Assuming a similar reflection coefficient for convection processes on Europa, Figs. 5b,c show that it is very likely that a 50-MHz instrument will penetrate a broad range of rigid lid thicknesses and allow characterization of the interface with the convecting layer beneath.

6. DISCUSSION AND CONCLUSIONS

There are strong scientific reasons for studying the subsurface structure of Europa's shell, especially as related to subsurface water and the nature of surface-ice-ocean exchange. The dielectric losses in very cold ice are low, yet highly sensitive to increasing temperature, water, and impurity content; therefore, much can be learned through orbital electromagnetic sounding of the icy shell. This is especially true when subsurface profiling is coupled to observations of both the topography and morphology of surface landforms and placed in the context of both surface composition and subsurface density distribution. Because of Jupiter's strong radio emissions and the unknown size of volume scatterers within Europa's icy shell, the range of sounding frequencies must be carefully matched to the science objectives. The thickness of Europa's icy shell is one of the most important questions left unanswered by Galileo. Determining the icy shell thickness is of fundamental astrobiological significance: It constrains the tidal heat the satellite is generating, whether the silicate interior is Io-like or not, and the means and extent to which the ocean and near-surface are likely to exchange material.

Science objectives for a radar sounder include characterizing the distribution of any shallow subsurface water; detecting the presence of a ice-ocean interface; correlating surface features and subsurface structure to investigate processes governing communication among the surface, icy shell, and ocean; and characterizing regional and global heat flow variations. The subsurface signatures from near-global surveys at high depth resolution combined with surface topography of similar vertical resolution would identify regions of possible ongoing or relatively recent upwelling of liquid water or brines. Orbital subsurface profiling of the top several kilometers of Europa's icy shell is possible, at frequencies slightly above the upper end of Jupiter's radio noise spectrum (i.e., about 40 MHz), to establish the geometry of various thermal, compositional, and structural horizons to a depth resolution of about 10 m (requiring a bandwidth of about 10 MHz). This high-resolution search for shallow water will produce data analogous to that of the SHARAD instrument.

Subsurface signatures from lower resolution but more deeply penetrating near-global surveys might reveal a shal-

low ice-ocean interface, which could be validated over a region by carefully correlating ice thickness and surface topography. An unequivocally thin icy shell, even within a limited region, would have significant implications for understanding direct exchange between the ocean and the overlying ice. Similarly, the detection of deep subsurface interfaces in these surveys and the presence or absence of shallower interfaces above them could validate hypotheses regarding the convective movement of deep ductile ice into the cold brittle shell implying indirect exchange with any ocean. Additional orbital profiling of the subsurface of Europa to depths approaching 30 km with a vertical resolution of about 100 m is recommended to establish the geometry of any deeper geophysical interfaces, in particular, to search for an ice-ocean interface. Although warm ice is very attenuating, "windows" of cold downwelling material may exist within the icy shell, allowing local penetration to great depths (*McKinnon,* 2005). Moreover, while the presence of meter-scale voids within the icy shell (*Eluszkiewicz,* 2004) would confound sounding efforts at higher frequencies (15 MHz), the presence of such large voids is probably unrealistic.

A deep ocean search would produce data analogous to that of MARSIS. Profiling could establish the geometry of any deeper geophysical interfaces that may correspond to an ice-ocean boundary to a vertical resolution of about 100 m (requiring a bandwidth of about 1 MHz). In particular, frequencies significantly less sensitive to any volume scattering that may be present in the shallow subsurface profiling detailed above (i.e., about 5 MHz) should be used on the antijovian side of Europa, which is substantially shadowed from Jupiter's radio emissions. This low-frequency, low-resolution profiling could complement high-frequency, low-resolution profiling over Europa's subjovian surface (where Jupiter's radio noise is an issue for low-frequency sounding).

Ultimately, observation campaigns targeted to specific features will be required to understand the processes controlling the distribution of any shallow subsurface water and either the direct or indirect exchange of materials between the icy shell and its underlying ocean. The presence of major cracks and faults as well as topographic and compositional anomalies, when correlated with subsurface structures within a particular targeted region, can provide critical information on tidal response and its role in subsurface fluid migration. Important factors include localized heating, the magnitude of tectonic stress, and associated strain release. Similarly, variations of the physical and compositional properties of the near-surface ice may arise because of relative age differences, tectonic deformation, mass wasting, or impact processes.

Because of the complex geometries expected for subsurface structures, full unprocessed subsurface imaging could be obtained along profiles at least 30 km long in any region of targeted study, either to a depth of several kilometers for high-resolution imaging of shallow targets or to a depth of tens of kilometers for lower-resolution imaging of deeper processes, in conjunction with co-located topographic measurements. These targeted subsurface studies would be a pathfinder for future *in situ* astrobiological exploration.

The thermal structure of the shell (apart from local heat sources) is set by the transport of heat from the interior. Regardless of the properties of the shell or the overall mechanism of heat transport, the uppermost several kilometers is thermally conductive, cold, and stiff. The thickness of this conductive "lid" is set by the total amount of heat that must be transported, and thus a measurement of the thickness of the cold and brittle part of the shell will provide a powerful constraint on the heat production in the interior. For a thin icy shell, the ice-ocean interface forms a significant dielectric horizon at the base of the thermally conductive layer.

However, when warm pure-ice diapirs from the interior of a thicker convective shell model approach the surface, they may be far from the pure-ice melting point and above the eutectic point of many substances and may therefore create regions of melting within the rigid shell above them as the temperature increases above the flattening diapir. Any dielectric horizon associated with these melt regions would also provide a good measurement of the thickness of the conductive layer. Global radar profiling of these subsurface thermal horizons to depths of tens of kilometers at a vertical resolution of 100 m will be vital in characterizing both regional and global heat flow variations in Europa's icy shell.

REFERENCES

Adams D. S. and Mobrem M. (2006) MARSIS antenna flight deployment anomaly and resolution. In *47th AIAA/ASME/ASCE/AHS/ASC Structures, Structural Dynamics, and Materials Conference,* No. 2006-1684. American Institute of Aeronautics and Astronautics, Newport, Rhode Island.

Bamber J. L. (1987) Internal reflecting horizons in Spitzbergen glaciers. *Ann. Glaciol., 9,* 5–10.

Bamber J. L. (1988) Enhanced radar scattering from water inclusions in ice. *J. Glaciol., 34(118),* 293–296.

Bell R. E., Studinger M., Tikku A. A., Clarke G. K. C., Gutner M. M., and Meertens C. (2002) Origin and fate of lake vostok water frozen to the base of the east antarctic ice sheet. *Nature, 416(6878),* 307–310.

Bentley C. R., Blankenship D. D., and Moline G. (1988) Electromagnetic studies on the siple coast, 1987–1988. *Antarc. J. U.S., 23(5),* 59.

Bentley C. R., Lord N., and Liu C. (1998) Radar reflections reveal a wet bed beneath stagnant Ice Stream C and a frozen bed beneath ridge BC, West Antarctica. *J. Glaciol., 44(146),* 149–156.

Bigg E. K. (1964) Influence of the satellite Io on Jupiter's decametric emission. *Nature, 203(4949),* 1008–1010, DOI:10.1038/2031008a0.

Bingham R. G. and Siegert M. J. (2007) Radio-echo sounding over polar ice masses. *J. Environ. Engineer. Geophys., 12(1),* 47–62, DOI: 10.2113/JEEG12.1.47.

Black G. J., Campbell D. B., and Ostro S. J. (2001) Icy galilean satellites: 70 cm radar results from Arecibo. *Icarus, 151,* 160–166, DOI: 10.1006/icar.2001.6615.

Blankenship D. D., Edwards B. C., Kim Y, Geissler P. E., Gurnett D. A., Johnson W. T. K., Kofman W. , Moore J. C., Morse D. L., Pappalardo R. T., Picardi G. , Raney R. K., Rodriguez

E. R., Shao X.-M., Weertman J. , Zebker H. A., and van Zyl J. (1999) *Feasibility Study and Design Concept for an Orbiting Ice-Penetrating Radar Sounder to Characterize in Three-Dimensions the Europan Ice Mantle Down to (and Including) any Ice/Ocean Interface.* Tech. Rept. 184, University of Texas Institute for Geophysics, Austin.

Blankenship D. D., Morse D., Finn C. A., Bell R. E., Peters M. E., Kempf S. D., Hodge S. M., Studinger M., Behrendt J. C., and Brozena J. M. (2001) Geological controls on the initiation of rapid basal motion for West Antarctic Ice Streams: A geophysical perspective including new airborne radar sounding and laser altimetry results. In *The West Antarctic Ice Sheet: Behavior and Environment* (R. B. Alley and R. A. Bindschadler, eds.), pp. 105–121. Antarctic Research Series, Vol. 77, American Geophysical Union, Washington, DC.

Blindow N. (1994) The central part of the Filchner-Ronne ice shelf, Antarctica: Internal structures revealed by 40 MHz monopulse RES. *Ann. Glaciol., 20,* 365–371.

Burke B. F. and Franklin K. L. (1955) Observations of a variable radio source associated with the planet Jupiter. *J. Geophys. Res., 60(2),* 213–217.

Campbell B. A. (2002) *Radar Remote Sensing of Planetary Surfaces*. Cambridge Univ., Cambridge.

Campbell B. A. and Shepard M. K. (2003) Coherent and incoherent components in near-nadir radar scattering: Applications to radar sounding of Mars. *J. Geophys. Res., 108(E12),* 5132, DOI: 10.1029/2003JE002164.

Cane H. V. (1979) Spectra of the non-thermal radio radiation from the galactic polar regions. *Mon. Not. R. Astron. Soc., 189,* 465–478.

Carter S. P., Blankenship D. D., Peters M. E., Young D. A., Holt J. W., and Morse D. L. (2007) Radar-based subglacial lake classification in Antarctica. *Geochem. Geophys. Geosys., 8,* Q03016, DOI: 10.1029/2006GC001408.

Catania G. A., Conway H., Gades A. M., Raymond C. F., and Engelhardt H. (2003) Bed reflectivity beneath inactive ice streams in West Antarctica. *Ann. Glaciol., 36,* 287–291.

Chyba C. F., Ostro S. J., and Edwards B. C. (1998) Radar detectability of a subsurface ocean on Europa. *Icarus, 134,* 292–302, DOI: 10.1006/icar.1998.5961.

Corr H. F. J. and Vaughan D. G. (2008) A recent volcanic eruption beneath the West Antarctic ice sheet. *Nature Geosci., 1,* 122–125, DOI: 10.1038/ngeo106.

Corr H., Moore J. C., and Nicholls K. W. (1993) Radar absorption due to impurities in Antarctic ice. *Geophys. Res. Lett., 20,* 1071–1074.

De Angelis M., Petit J. R., Savarino J., Souchez R., and Thiemens M. H. (2004) Contributions of an ancient evaporitic-type reservoir to subglacial Lake Vostok chemistry. *Earth Planet. Sci. Lett., 222(3–4),* 751–765.

Dowdeswell J. A. and Evans S. (2004) Investigations of the form and flow of ice sheets and glaciers using radio-echo sounding. *Rept. Progr. Phys., 67,* 1821–1861, DOI: 10.1088/0034-4885/67/10/R03.

Dulk G. A., Erickson W. C., Manning R., and Bougeret J.-L. (2001) Calibration of low-frequency radio telescopes using the galactic background radiation. *Astron. Astrophys., 365(2),* 294–300, DOI: 10.1051/0004-6361:20000006.

Elachi C., Wall S., Allison M., Anderson Y., Boehmer R., Callahan P., Encrenaz P., Flamini E., Franceschetti G., Gim Y., Hamilton G., Hensley S., Janssen M., Johnson W., Kelleher K., Kirk R., Lopes R., Lorenz R., Lunine J., Muhleman D., Ostro S., Paganelli F., Picardi G., Posa F., Roth L., Seu R., Shaffer S., Soderblom L., Stiles B., Stofan E., Vetrella S., West R., Wood C., Wye L., and Zebker H. (2005) Cassini radar views the surface of Titan. *Science, 308(5724),* 970–974.

Eluszkiewicz J. (2004) Dim prospects for radar detection of Europa's ocean. *Icarus, 170,* 234–236, DOI: 10.1016/j.icarus.2004.02.011.

Engelhardt H. and Determann J. (1987) Borehole evidence for a thick layer of basal ice in the central Ronne Ice Shelf. *Nature, 327(6120),* 318–319.

Evans S. (1961) Polar ionospheric spread echoes and radio frequency properties of ice shelves. *J. Geophys. Res., 66(12),* 4137–4141.

Evans S. (1965) Dielectric properties of ice and snow — A review. *J. Glaciol., 5,* 773–793.

Eviatar A., Siscoe G. L., Johnson T. V., and Matson D. L. (1981) Effects of Io ejecta on Europa. *Icarus, 47,* 75–83, DOI: 10.1016/0019-1035(81)90092-0.

Figueredo P. H. and Greeley R. (2004) Resurfacing history of Europa from pole-to-pole geologic mapping. *Icarus, 167,* 287–312, DOI: 10.1016/j.icarus.2003.09.016.

Franceschetti G. and Lanari R. (1999) *Synthetic Aperture Radar Processing.* CRC Press, Boca Raton, Florida.

Fricker H. A., Popov S., Allison I., and Young N. (2001) Distribution of marine ice beneath the Amery ice shelf. *Geophys. Res. Lett., 28(11),* 2241–2244, DOI: 10.1027/2000GL012461.

Fricker H. A., Scambos T., Bindschadler R., and Padman L. (2007) An active subglacial water system in West Antarctica mapped from space. *Science, 315(5818),* 1544–1548, DOI: 10.1126/science.1136897.

Fujita S., Matsuoka T., Morishima S., and Mae S. (1993) The measurement on the dielectric properties of ice at HF, VHF and microwave frequencies. In *Geoscience and Remote Sensing Symposium, 1993. IGARSS '93. Better Understanding of Earth Environment, International,* pp. 1258–1260, DOI: 10.1109/IGARSS.1993.322667.

Gades A. M., Raymond C. F., Conway H., and Jacobel R. W. (2000) Bed properties of Siple Dome and adjacent ice streams, West Antarctica, inferred from radio-echo sounding measurements. *J. Glaciol., 46(152),* 88–94, DOI: 10.3189/172756500781833467.

Giese B., Oberst J., Roatsch T., Neukum G., Head J. W., and Pappalardo R. T. (1998) The local topography of Uruk Sulcus and Galileo Regio obtained from stereo images. *Icarus, 135(1),* 303–316, DOI: 10.1006/icar.1998.5967.

Glen J. W. and Paren J. G. (1975) The electrical properties of snow and ice. *J. Glaciol., 15,* 15–37.

Gogineni S., Tammana D., Braaten D., Leuschen C., Akins T., Legarsky J., Kanagaratnam P., Stiles J., Allen C., and Jezek K. (2001) Coherent radar ice thickness measurements over the Greenland ice sheet. *J. Geophys. Res., 106(D24),* 33761–33772, DOI: 10.1027/2001JD900183.

Gogineni S., Braaten D., Allen C., Paden J., Akins T., Kanagaratnam P., Jezek K., Prescott G., Jayaraman G., Ramasami V., Lewis C., and Dunson D. (2007) Polar Radar for Ice Sheet Measurements (PRISM). *Remote Sensing Environ., 111(2–3),* 204–211.

Greenberg R., Geissler P., Hoppa G., Tufts B. R., Durda D. D., Pappalardo R., Head J. W., Greeley R., Sullivan R., and Carr M. H. (1998) Tectonic processes on Europa: Tidal stresses, mechanical response, and visible features. *Icarus, 135,* 64–78, DOI: 10.1006/icar.1998.5986.

Greenberg R., Hoppa G. V., Tufts B. R., Geissler P., Riley J., and Kadel S. (1999) Chaos on Europa. *Icarus, 141,* 263–286, DOI: 10.1006/icar.1999.6187.

Greenberg R., Geissler P., Hoppa G., and Tufts B. R. (2002) Tidal-tectonic processes and their implications for the character of Europa's icy crust. *Rev. Geophys., 40,* 1–1, DOI: 10.1029/2000RG000096.

Gross G. W., Hayslip I. C., and Hoy R. N. (1978) Electrical conductivity and relaxation in ice crystals with known impurity content. *J. Glaciol., 21(85),* 143–160.

Gudmandsen P. (1971) Electromagnetic probing of ice. In *Electromagnetic Probing in Geophysics* (J. R. Wait, ed.), pp. xx–yy. Golem Press, Colorado.

Hand K. P. and Chyba C. F. (2007) Empirical constraints on the salinity of the europan ocean and implications for a thin ice shell. *Icarus, 189(2),* 424–438, DOI: 10.1016/j.icarus.2007.02.002.

Heliere F., Lin C.-C., Corr H., and Vaughan D. (2007) Radio echo sounding of Pine Island Glacier, West Antarctica: Aperture synthesis processing and analysis of feasibility from space. *IEEE Trans. Geosci. Remote Sensing, 45(8),* 2573–2582, DOI: 10.1109/TGRS.2007.897433.

Holt J. W., Peters M. E., Kempf S. D., Morse D. L., and Blankenship D. D. (2006a) Echo source discrimination in single-pass airborne radar sounding data from the Dry Valleys, Antarctica: Implications for orbital sounding of Mars. *J. Geophys. Res., 111(E10),* DOI: 10.1029/2005JE002525.

Holt J. W., Peters M. E., Morse D. L., Blankenship D. D., Lindzey L. E., Kavanaugh J. L., and Cuffey K. M. (2006b) Identifying and characterizing subsurface echoes in airborne radar sounding data from a high clutter environment in Taylor Valley, Antarctica. In *11th International Conference on Ground Penetrating Radar,* June 19–22, Columbus, Ohio.

Hoppa G. V., Tufts B. R., Greenberg R., and Geissler P. E. (1999) Formation of cycloidal features on Europa. *Science, 285,* 1899–1902.

Jacobel R. W. and Welch B. C. (2006) A time marker at 17.5 k.y. BP detected throughout West Antarctica. *Ann. Glaciol., 41(1),* 47–51.

Jezek K. C., Rodrìguez E., Gogineni P., Freeman A., Curlandr J., Wu X., Paden J., and Allen C. (2006) Glaciers and ice sheets mapping orbiter concept. *J. Geophys. Res., 111(E06S20),* DOI: 10.1029/2005JE002572.

Kargel J. S. (1991) Brine volcanism and the interior structures of asteroids and icy satellites. *Icarus, 94(2),* 368–390, DOI: 10.1016/0019-1035(91)90235-L.

Kivelson M. G., Khurana K. K., Russell C. T., Volwerk M., Walker R. J., and Zimmer C. (2000) Galileo magnetometer measurements: A stronger case for a subsurface ocean at Europa. *Science, 289,* 1340–1343.

Kurth W. S., Gurnett D. A., Persoon A. M., Roux A., Bolton S. J., and Alexander C. J. (2001) The plasma wave environment of Europa. *Planet. Space Sci., 49,* 345–363, DOI: 10.1016/S0032-0633(00)00156-2.

Lee S., Pappalardo R. T., and Makris N. C. (2005), Mechanics of tidally driven fractures in Europa's ice shell. *Icarus, 177,* 367–379, DOI: 10.1016/j.icarus.2005.07.003.

Legarsky J. J., Gogineni S. P., and Akins T. L. (2001) Focused synthetic aperture radar processing of ice-sounder data collected over the Greenland ice sheet. *Geosci. Remote Sensing, IEEE Trans., 39(10),* 2109–2117.

Lewis E. L. and Perkin R. G. (1986) Ice pumps and their rates. *J. Geophys. Res., 91(C10),* 11756–11762.

MacGregor J. A., Winebrenner D., Conway H., Matsuoka K., Mayewski P. A., and Clow G. (2007) Modeling englacial radar attenuation at Siple Dome, West Antarctica, using ice chemistry and temperature data. *J. Geophys. Res., 112(F03008),* DOI: 10.1029/2006JF000717.

McEwen A. S. (1986) Exogenic and endogenic albedo and color patterns on Europa. *J. Geophys. Res., 91,* 8077–8097.

McKinnon W. B. (2005) Radar sounding of convecting ice shells in the presence of convection: Application to Europa, Ganymede, and Callisto. In *Workshop on Radar Investigations of Planetary and Terrestrial Environments,* Abstract #6039. Lunar and Planetary Institute, Houston.

McKinnon W. B. and Zolensky M. E. (2003) Sulfate content of Europa's ocean and shell: Evolutionary considerations and some geological and astrobiological implications. *Astrobiology, 3,* 879–897, DOI: 10.1089/153110703322736150.

Moore J. C. (2000) Models of radar absorption in europan ice. *Icarus, 147(1),* 292–300, DOI: 10.1006/icar.2000.6425.

Moore J. C., Paren J. G., and Oerter H. (1992) Sea salt dependent electrical conduction in polar ice. *J. Geophys. Res., 97(B13),* 19803–19812.

Moore J. C., Reid A. P., and Kipfstuhl J. (1994) Microstructure and electrical properties of marine ice and its relationship to meteoric ice and sea ice. *J. Geophys. Res., 99(C3),* 5171–5180, DOI: 10.1029/93JC02832.

Moore J. M., Asphaug E., Sullivan R. J., Klemaszewski J. E., Bender K. C., Greeley R., Geissler P. E., McEwen A. S., Turtle E. P., Phillips C. B., Tufts B. R., Head J. W., Pappalardo R. T., Jones K. B., Chapman C. R., Belton M. J. S., Kirk R. L., and Morrison D. (1998) Large impact features on Europa: Results of the Galileo nominal mission. *Icarus, 135,* 127–145, DOI: 10.1006/icar.1998.5973.

Musil G. J. and Doake C. S. M. (1987) Imaging subglacial topography by a synthetic aperture technique. *Ann. Glaciol., 9,* 170–175.

Neal C. S. (1979) The dynamics of the Ross ice shelf revelad by radio echo sounding. *J. Glaciol., 24(90),* 295–307.

Nimmo F. and Gaidos E. (2002) Strike-slip motion and double ridge formation on Europa. *J. Geophys. Res.–Planets, 107,* 5021, DOI: 10.1029/2000JE001476.

Nimmo F. and Manga M. (2002) Causes, characteristics and consequences of convective diapirism on Europa. *Geophys. Res. Lett., 29(23),* 2109, DOI: 10.1029/2002GL015754.

Nimmo F. and Schenk P. (2008) Stereo and photoclinometric comparisons and topographic roughness of Europa. In *Lunar and Planetary Science XXXIX,* Abstract #1464. Lunar and Planetary Institute, Houston (CD-ROM).

Nouvel J. F., Herique A., Kofman W., and Safaeinili A. (2004) Radar signal simulation: Surface modeling with the Facet Method. *Radio Science, 39,* RS1013, DOI: 10.1029/2003RS002903.

Oliason S. and Falola B. (2001) *Ice Thickness Interpretation Over Lake Vostok, Antarctica.* Applied Research Laboratories Technical Report ARL-LR-DO-01-01, The University of Texas at Austin.

Ono T., Kumamoto A., Yamaguchi Y., Yamaji A., Kobayashi T., Kasahara Y., and Oya H. (2008) Instrumentation and observation target of the Lunar Radar Sounder (LRS) experiment onboard the SELENE spacecraft. *Earth Planets Space, 60(4),* 321–332.

Ostro S. J. and Shoemaker E. M. (1990) The extraordinary radar echoes from Europa, Ganymede, and Callisto — A geological perspective. *Icarus, 85,* 335–345, DOI: 10.1016/0019-1035(90)90121-O.

Ostro S. J., West R. D., Janssen M. A., Lorenz R. D., Zebker H. A., Black G. J., Lunine J. I., Wye L. C., Lopes R. M., Wall S. D., Elachi C., Roth L., Hensley S., Kelleher K., Hamilton

G. A., Gim Y., Anderson Y. Z., Boehmer R. A., and Johnson W. T. K. (2006) Cassini RADAR observations of Enceladus, Tethys, Dione, Rhea, Iapetus, Hyperion, and Phoebe. *Icarus, 183(2),* 479–490, DOI: 10.1016/j.icarus.2006.02.019.

Pälli A., Moore J. C., and Rolstad C. (2003) Firn-ice transition zones of polythermal glaciers. *Ann. Glaciol., 37,* 298–304.

Pappalardo R. T. and Barr A. C. (2004) The origin of domes on Europa: The role of thermally induced compositional diapirism. *Geophys. Res. Lett., 31,* 1701, DOI: 10.1029/2003GL019202.

Pappalardo R. T. and Sullivan R. J. (1996) Evidence for separation across a gray band on Europa. *Icarus, 123,* 557–567, DOI: 10.1006/icar.1996.0178.

Pappalardo R. T., Head J. W., Greeley R., Sullivan R. J., Pilcher C., Schubert G., Moore W. B., Carr M. H., Moore J. M., Belton M. J. S., and Goldsby D. L. (1998) Geological evidence for solid-state convection in Europa's ice shell. *Nature, 391,* 365, DOI: 10.1038/34862.

Pappalardo R. T., Belton M. J. S., Breneman H. H., Carr M. H., Chapman C. R., Collins G. C., Denk T., Fagents S., Geissler P. E., Giese B., Greeley R., Greenberg R., Head J. W., Helfenstein P., Hoppa G., Kadel S. D., Klaasen K. P., Klemaszewski J. E., Magee K., McEwen A. S., Moore J. M., Moore W. B., Neukum G., Phillips C. B., Prockter L. M., Schubert G., Senske D. A., Sullivan R. J., Tufts B. R., Turtle E. P., Wagner R., and Williams K. K. (1999) Does Europa have a subsurface ocean? Evaluation of the geological evidence. *J. Geophys. Res., 104,* 24015–24056, DOI: 10.1029/1998JE000628.

Paterson W. S. B. (1994) *The Physics of Glaciers,* 3rd edition, Butterworth Heinmann.

Peake W. H. and Barrick D. E. (1967) *Scattering from Surface with Different Roughness Scales: Analysis and Interpretation.* ElectroScience Laboratory Publication 1388-26, Ohio State University.

Peters M. E., Blankenship D. D., and Morse D. L. (2005) Analysis techniques for coherent airborne radar sounding: Application to West Antarctic ice streams. *J. Geophys. Res., 110(B06303),* DOI: 10.1029/2004JB003222.

Peters M. E., Blankenship D. D., Carter S. P., Young D. A., Kempf S. D., and Holt J. W. (2007a) Along-track focusing of airborne radar sounding data from West Antarctica for improving basal reflection analysis and layer detection. *IEEE Trans. Geosci. Remote Sensing, 45(9),* 2725–2736, DOI: 10.1109/TGRS.2007.897416.

Peters M. E., Blankenship D. D., Smith D. E., Holt J. W., and Kempf S. D. (2007b) The distribution and classification of bottom crevasses from radar sounding of a large tabular iceberg. *Geosci. Remote Sensing Lett., IEEE, 4(1),* 142–146.

Petrenko V. F. and Whitworth R. W. (1999) *Physics of Ice.* Oxford Univ., New York.

Phillips R. J., Zuber M. T., Smrekar S. E., Mellon M. T., Head J. W., Tanaka K. L., Putzig N. E., Milkovich S. M., Campbell B. A., Plaut J. J., Safaeinili A., Seu R., Biccari D., Carter L. M., Picardi G., Orosei R., Mohit P. S., Heggy E., Zurek R. W., Egan A. F., Giacomoni E., Russo F., Cutigni M., Pettinelli E., Holt J. W., Leuschen C. J., and Marinangeli L. (2008) Mars north polar deposits: Stratigraphy, age, and geodynamical response. *Science, 320(5880),* 1182–1185, DOI: 10.1126/science.1157546.

Picardi G., Plaut J. J., Biccari D., Bombaci O., Calabrese D., Cartacci M., Cicchetti A., Clifford S. M., Edenhofer P., Farrell W. M., Federico C., Frigeri A., Gurnett D. A., Hagfors T., Heggy E., Herique A., Huff R. L., Ivanov A. B., Johnson W. T. K., Jordan R. L., Kirchner D. L., Kofman W., Leuschen C. J., Nielsen E., Orosei R., Pettinelli E., Phillips R. J., Plettemeier D., Safaeinili A., Seu R., Stofan E. R., Vannaroni G., Watters T. R., and Zampolini E. (2005) Radar soundings of the subsurface of Mars. *Science, 310(5756),* 1925–1928.

Plaut J. J., Picardi G., and the MARSIS Team (2007) One Mars year of MARSIS observations: Global reconnaissance of the subsurface and ionosphere of Mars. In *Seventh International Conference on Mars,* Abstract #3341, Lunar and Planetary Institute, Houston (CD-ROM).

Porcello L. J., Jordan R. L., Zelenka J. S., Adams G. F., Phillips R. J., Brown W. E. Jr., Ward S. H., and Jackson P. L. (1974) The Apollo lunar sounder radar system. *Proc. IEEE, 62(6),* 769–783.

Robin G., Drewry D. J., and Meldrum D. T. (1977) International studies of ice sheet and bedrock. *Philos. Trans. R. Soc. B, 279,* 185–196.

Robin G., Doake C. S. M., Kohnen H., Crabtree R. D., Jordan S. R., and Moller D. (1983) Regime of the Filchner-Ronne ice shelves, Antarctica. *Nature, 302(5909),* 582–586.

Saunders R. S., Spear A. J., Allin P. C., Austin R. S., Berman A. L., Chandlee R. C., Clark J. , deCharon A. V., de Jong E. M., Griffith D. G., Gunn J. M., Hensley S., Johnson W. T. K., Kirby C. E., Leung K. S., Lyons D. T., Michaels G. A., Miller J., Morris R. B., Morrison A. D., Piereson R. G., Scott J. F., Shaffer S. J., Slonski J. P., Stofan E. R., Thompson T. W., and Wall S. D. (1992) Magellan mission summary. *J. Geophys. Res., 97(E8),* 13067–13090, DOI: 10.1029/92JE01397.

Schenk P. M. (2005) Landing site characteristics for Europa 1: Topography. In *Lunar and Planetary Science XXXVI,* Abstract #2321. Lunar and Planetary Institute, Houston (CD-ROM).

Schenk P. M. and McKinnon W. B. (1989) Fault offsets and lateral crustal movement on Europa — Evidence for a mobile ice shell. *Icarus, 79,* 75–100, DOI: 10.1016/0019-1035(89)90109-7.

Schenk P. M. and Pappalardo R. T. (2004) Topographic variations in chaos on Europa: Implications for diapiric formation. *Geophys. Res. Lett., 31,* 16703, DOI: 10.1029/2004GL019978.

Schenk P., Matsuyama I., and Nimmo F. (2008) True polar wander on Europa from global-scale small-circle depressions. *Nature, 453(7193),* 368–371.

Seu R., Phillips R. J., Biccariy D., Orosei R., Masdea A., Picardi G., Safaeinili A., Campbell B. A., Plaut J. J., Marinangeli L. , Smrekar S. E., and Nunes D. C. (2007) SHARAD sounding radar on the Mars Reconnaissance Orbiter. *J. Geophys. Res., 112(E05S05),* DOI: 10.1029/2006JE002745.

Shabtaie S. and Bentley C. R. (1987) West Antarctic ice streams draining into the Ross Ice Shelf: Configuration and mass balance. *J. Geophys. Res., 92(B2),* 1311–1336.

Shepard M. K., Campbell B. A., Bulmer M. H., Farr T. G., Gaddis L. R., and Plaut J. J. (2001) The roughness of natural terrain: A planetary and remote sensing perspective. *J. Geophys. Res., 106(E12),* 32777–32795, DOI: 1029/2001JE001429.

Siegert M. J. (2005) Lakes beneath the ice sheet: The occurrence, analysis, and future exploration of Lake Vostok and other Antarctic subglacial lakes. *Annu. Rev. Earth Planet. Sci., 33(1),* 215–245, DOI: 10.1146/annurev.earth.33.092203.122725.

Souchez R., Jean-Baptiste P., Petit J. R., Lipenkov V. Y., and Jouzel J. (2003) What is the deepest part of the Vostok ice core telling us? *Earth Sci. Rev., 60(1–2),* 131–146, DOI: 10.1016/S0012-8252(02)00090-9.

Souchez R., Petit J. R., Jouzel J., de Angelis M., and Tison J. L. (2004) Reassessing Lake Vostok's behaviour from existing and new ice core data. *Earth Planet. Sci. Lett., 217(1–2),* 163–170.

Spikes V. B., Hamilton G. S., Arcone S. A., Kaspari S., and

Mayewski P. A. (2004) Variability in accumulation rates from GPR profiling on the West Antarctic plateau. *Ann. Glaciol., 39(1),* 238–244.

Squyres S. W., Reynolds R. T., and Cassen P. M. (1983) Liquid water and active resurfacing on Europa. *Nature, 301,* 225, DOI: 10.1038/301225a0.

Stiles B., Gim Y., Hamilton G., Hensley S., Johnson W., Shimada J., West R., and Callahan P. (2006) Ground processing of Cassini RADAR imagery of Titan. In *2006 IEEE Conference on Radar,* p. 8, DOI: 10.1109/RADAR.2006.1631767.

Thyssen F. (1998) Special aspects of the central part of Filchner-Ronne Ice Shelf, Antarctic. *Ann. Glaciol., 11,* 173–179.

Waite A. and Schmidt S. (1962) Gross errors in height indication from pulsed radar altimeters operating over thick ice or snow. *Proc. Inst. Radio Engineers, 50(6),* 1515–1520, DOI: 10.1109/JRPROC.1962.288195.

Weeks W. F., Gow A. J., Kosloff P., and Digby-Argus S. (1990) The internal structure, compostion and properties of brackish ice from the Bay of Bothnia. In *Sea Ice Properties and Processes* (S. F. Ackley and W. F. Weeks, eds.), pp. 5–15. CRREL Monograph 90.

Wye L. C., Zebker H. A., Ostro S. J., West R. D., Gim Y., Lorenz R. D., and the Cassini RADAR Team (2007) Electrical properties of Titan's surface from Cassini RADAR scatterometer measurements. *Icarus, 188(2),* 367–385, DOI: 10.1016/j.icarus.2006.12.008.

Zahnle K., Schenk P., Levison H., and Dones L. (2003) Cratering rates in the outer solar system. *Icarus, 163(2),* 263–289.

Zarka P. (2004) Fast radio imaging of Jupiter's magnetosphere at low-frequencies with LOFAR. *Planet. Space Sci., 52(15),* 1455–1467, DOI: 10.1016/j.pss.2004.09.017.

Zarka P., Cecconi B., and Kurth W. S. (2004) Jupiter's low-frequency radio spectrum from Cassini/Radio and Plasma Wave Science (RPWS) absolute flux density measurements. *J. Geophys. Res., 109(A09S15),* DOI: 10.1029/2003JA010260.

Zolotov M. Y. and Shock E. L. (2001) Composition and stability of salts on the surface of Europa and their oceanic origin. *J. Geophys. Res., 106,* 32815–32828, DOI: 10.1029/2000JE001413.